The Astrophysical Journal Supplement Series, 229:39 (16pp), 2017 April https://doi.org/10.3847/1538-4365/aa6971

A Catalog of Narrow Line Seyfert 1 Galaxies from the Sloan Digital Sky Survey Data Release 12

Suvendu Rakshit[1], C. S. Stalin[1], Hum Chand [2], and Xue-Guang Zhang [3]
[1] Indian Institute of Astrophysics, Block II, Koramangala, Bangalore-560034, India; suvenduat@gmail.com
[2] Aryabhatta Research Institute of Observational Sciences (ARIES), 263002, Nainital, India
[3] Institute of Astronomy and Space Science, Sun Yat-Sen University, No. 135, Xingang Xi Road, Guangzhou, 510275, P. R. China
Received 2016 October 1; revised 2017 February 11; accepted 2017 March 3; published 2017 April 17

Abstract

We present a new catalog of narrow-line Seyfert 1 (NLSy1) galaxies from the Sloan Digital Sky Survey Data Release 12 (SDSS DR12). This was obtained by a systematic analysis through modeling of the continuum and emission lines of the spectra of all the 68,859 SDSS DR12 objects that are classified as "QSO" by the SDSS spectroscopic pipeline with $z < 0.8$ and a median signal-to-noise ratio $(S/N) > 2\,\mathrm{pixel}^{-1}$. This catalog contains a total of 11,101 objects, which is about 5 times larger than the previously known NLSy1 galaxies. Their monochromatic continuum luminosity at 5100 Å is found to be strongly correlated with Hβ, Hα, and [O III] emission line luminosities. The optical Fe II strength in NLSy1 galaxies is about two times larger than the broad-line Seyfert 1 (BLSy1) galaxies. About 5% of the catalog sources are detected in the FIRST survey. The Eddington ratio (ξ_{Edd}) of NLSy1 galaxies has an average of $\log \xi_{\mathrm{Edd}}$ of -0.34, much higher than -1.03 found for BLSy1 galaxies. Their black hole masses (M_{BH}) have an average of $\log M_{\mathrm{BH}}$ of 6.9 $M_{\odot}$, which is less than BLSy1 galaxies, which have an average of $\log M_{\mathrm{BH}}$ of 8.0 $M_{\odot}$. The M_{BH} of NLSy1 galaxies is found to be correlated with their host galaxy velocity dispersion. Our analysis suggests that geometrical effects playing an important role in defining NLSy1 galaxies and their M_{BH} deficit is perhaps due to their lower inclination compared to BLSy1 galaxies.

Key words: galaxies: active – galaxies: Seyfert – techniques: imaging spectroscopy

Supporting material: machine-readable table

1. Introduction

Seyfert galaxies, a type of active galactic nuclei (AGNs) are generally classified into two broad categories depending on their emission line properties; namely Seyfert 1 (Sy 1) and Seyfert 2 (Sy 2) galaxies (see Netzer 2015). Traditionally, an AGN is termed a Seyfert galaxy or a quasar when its absolute optical magnitude is fainter or brighter than a (somewhat arbitrary) value, e.g., $M_B = -23$ (Véron-Cetty & Véron 2010). Sy 1 galaxies show both broad permitted emission lines that originate from the broad-line region (BLR) having widths of a few thousand km s^{-1} and narrow forbidden emission lines that originate from the narrow line region (NLR) and having widths of a few hundred km s^{-1}. On the other hand, Sy 2 galaxies show narrow permitted and forbidden lines in their emission line spectra (Robson 1996). The varied observational differences seen between Sy 1 and Sy 2 galaxies are explained by unification model (Antonucci 1993), according to which, both of them have similar internal structure and the differences in their spectra are mainly due to orientation effects. The narrow lines seen in the spectra of Sy 2 galaxies are due to the fact that they are viewed close to edge-on and becuase the view of their BLR is obscured by the torus. However, based on recent observations, Netzer (2015) concluded that the simple unification scheme requires some major modifications.

Although the division between Seyfert galaxies is well defined, exceptions have been found. Some Seyfert galaxies show narrow "broad permitted lines" similar to the Sy 2 galaxies, though they have all the spectral properties of Sy 1 sources. They were classified as narrow-line Seyfert 1 (NLSy1) galaxies by Osterbrock & Pogge (1985), initially based on the presence of narrow permitted emission lines and weak [O III] lines relative to Hβ with [O III]λ5007/H$\beta < 3$. Later, Goodrich (1989) put an upper limit on the width of the permitted lines, the full width at half maximum (FWHM) of the broad Hβ line <2000 km s^{-1}, to quantitatively define the NLSy1 category. NLSy1 galaxies often show strong Fe II emission lines relative to Hβ in the UV and optical spectral domain, a strong soft X-ray excess, and high amplitude rapid X-ray variability (Boller et al. 1996; Leighly 1999). In the soft X-ray band, NLSy1 galaxies have a photon index of $\Gamma = 2.19 \pm 0.10$ (Leighly 1999), which is significantly steeper than the broad-line Seyfert 1 (BLSy1) galaxies (Nandra & Pounds 1994). They are generally believed to have lower black hole masses (10^6–$10^8\,M_{\odot}$) and higher Eddington ratios than BLSy1 galaxies (Zhou et al. 2006, hereafter ZH06) since the former have narrower Balmer lines than the latter (see also Xu et al. 2012). However, there are reports that the black hole masses of NLSy1 and BLSy1 galaxies are indifferent, and geometrical effects can fully account for the mass deficit in NLSy1 galaxies (Calderone et al. 2013; Baldi et al. 2016; Liu et al. 2016). A majority of the population of NLSy1 galaxies are radio quiet with a minority of about 7% are known to be radio loud (Pogge 2000). The radio-loud fraction of NLSy1 galaxies is indeed half of the 15% that we know for the quasar category of AGNs (Kellermann et al. 1989).

One of the many correlations that drive the eigenvector 1 (E1) in AGNs is the strong anti-correlation between Fe II emission and [O III] line strength (Boroson & Green 1992; Grupe et al. 1999; McIntosh et al. 1999). Interestingly, NLSy1 galaxies lie at the extremely low [O III] or negative end of E1, providing a unique opportunity to study the physical parameters responsible for such an unusual class. The drivers of E1 are expected to be

the black hole mass, accretion rate, orientation angle, and covering factor or anisotropy of the BLR (Boroson & Green 1992; Wang et al. 1996; Boroson 2002). Recently, Shen & Ho (2014) showed that the main driving physical parameters of E1 in AGNs are the Eddington ratio and orientation that affect the observed line profile.

The number of NLSy1 galaxies has gradually increased in the last two decades. From the Sloan Digital Sky Survey (SDSS) early data release, Williams et al. (2002) compiled a catalog of 150 NLSy1 galaxies. This number increased to 2011 sources, when SDSS DR3 was used by ZH06. There is an about a factor of 10 increase in the number of AGNs in SDSS spectroscopic data release 12 (SDSS DR12 Alam et al. 2015) than in DR3, offering the identification of a large sample of new NLSy1 galaxies. The main motivation for this work is therefore to increase the number of NLSy1 galaxies we know today, using the enlarged list of sources from SDSS DR12. The finding of a large sample of NLSy1 galaxies from a systematic analysis of SDSS DR12 spectra could allow us to study their properties, in general, and to verify the previously known correlations and establish new correlations on various physical properties of these sources. Toward this goal, we have systematically searched for NLSy1 galaxies in the spectroscopic "QSO" sample of SDSS DR12. In this work, we present this new catalog of NLSy1 galaxies and the results of various analyses carried out on this new sample to understand their properties. This paper is organized as follows. In Section 2, we present the data sets used for searching NLSy1 galaxies and describe the spectral analysis procedure. The sample of NLSy1 galaxies is presented in Section 3 and their properties are discussed in Section 4. A summary of the key results of the work is given in Section 5. A cosmology with $H_0 = 70\ \mathrm{km\ s^{-1}\ Mpc^{-1}}$, $\Omega_m = 0.3$, and $\Omega_\lambda = 0.7$ is assumed throughout.

2. Data and Spectral Analysis

We selected objects from the "specObj"[4] data product of the SDSS DR12 catalog (Alam et al. 2015) that are classified as "QSO" by the SDSS spectroscopic pipeline (Richards et al. 2002; Ross et al. 2012). This can include both SDSS and Baryon Oscillation Spectroscopic Survey (BOSS; Dawson et al. 2013) spectra with a wavelength coverage of λ3800–9200 Å and λ3600–10400 Å respectively. However, to ensure the presence of both Hβ and [O III] emission lines within the wavelength coverage of SDSS and BOSS spectra as well as for the convenience of comparison to ZH06, we considered objects with $z < 0.8$. This yielded 114,806 sources, of which only sources that have a median signal-to-noise ratio $(\mathrm{S/N}) > 2\ \mathrm{pixel^{-1}}$ were retained. This resulted in 68,859 sources that were taken further for a detailed spectral analysis.

To carefully analyze the spectra and accurately estimate the emission line parameters, we performed a two-step fitting process (see also, Zhang 2014; Zhang & Feng 2016) after shifting the spectra to their rest frame.

I. The spectra were simultaneously fitted with an AGN power-law continuum (global) and stellar contribution of host galaxy using Equation (1). During this step, we masked the AGN emission lines except Fe II multiplets (see Section 2.1). We then subtracted the stellar contribution from the spectra without subtracting the AGN global continuum, and proceeded to the next step given below.
II. In this step, we simultaneously fitted AGN emission lines including local AGN continuum along with Fe II template to the host galaxy subtracted spectra obtained in Step I above (see Section 2.2). From this fitting, we estimated all the emission line and continuum parameters of AGNs.

2.1. Subtraction of Host Contribution

The spectra of low-redshift AGNs may contain a significant contribution from the host galaxy starlight. To elucidate important information on AGN properties from the spectra, the stellar light contribution needs to be removed. We used the simple stellar population (SSP) method to remove the contribution of host galaxy from the spectra and estimated the stellar properties following Zhang (2014) and Zhang & Feng (2016). The observed spectrum, $F(\lambda)$, can be modeled using SSP method as follows:

$$F(\lambda) = \left[\sum_{i=1}^{39} a_i \times F_{\mathrm{ssp}}(\delta\lambda, r_\lambda)\right] * g(\lambda, \sigma_*) + F_{\mathrm{AGN}}(\lambda, r_\lambda), \quad (1)$$

where the first part of the right-hand side represents the contribution of host galaxy starlight and the second part represents the AGN contribution. Here a_i is the amplitude of the individual SSP templates, $F_{\mathrm{ssp}}(\delta\lambda, r_\lambda)$ is the SSP template with a wavelength shift of $\delta\lambda$ and reddening factor of r_λ, $g(\lambda, \sigma_*)$ is the Gaussian broadening function with velocity σ_* considered as the stellar velocity dispersion, and $F_{\mathrm{AGN}}(\lambda, r_\lambda)$ is the contribution from the AGN in the form of λ^α with the reddening correction factor r_λ (α is the power-law index). The summation runs from $i = 1$ to 39 as the SSP model is applied with 39 simple stellar template spectra. The templates were taken from Bruzual & Charlot (2003) having ages between 5 Myr and 12 Gyr and solar metallicities of $Z = 0.008$, 0.05, and 0.02. A detailed description of the SSP method is given in Bruzual & Charlot (2003), Kauffmann et al. (2003), Wang et al. (2009), Cappellari et al. (2012), and Zhang (2014).

We masked the emission lines without considering the Fe II multiplets as emission lines so as to leave sufficient continuum windows for continuum fitting and performed Levenberg–Marquardt least-squares minimization using *IDL mpfit*[5] fitting package (Markwardt 2009) to fit the spectra. This allowed us to decompose the contribution of the host galaxy and AGN continuum from the spectra. We then subtracted the contribution of the host galaxy stellar light from the spectra without subtracting AGN global continuum. Figure 1 shows examples of starlight subtraction from the spectra. The decomposed AGN continuum emission component is shown by a solid green line, host galaxy contribution is shown by a solid blue line. We note that the continuum fitting procedure is phenomenological, which is sufficient for the present study.

2.2. Emission Line Fitting

After subtracting the starlight contribution from the spectra as described above, we performed a simultaneous fitting of emission lines including one local power-law continuum

[4] "specObj" contains only the best spectra for any object obtained by SDSS (see http://www.sdss.org/dr12/help/faq/#scienceprimary).

[5] http://purl.com/net/mpfit

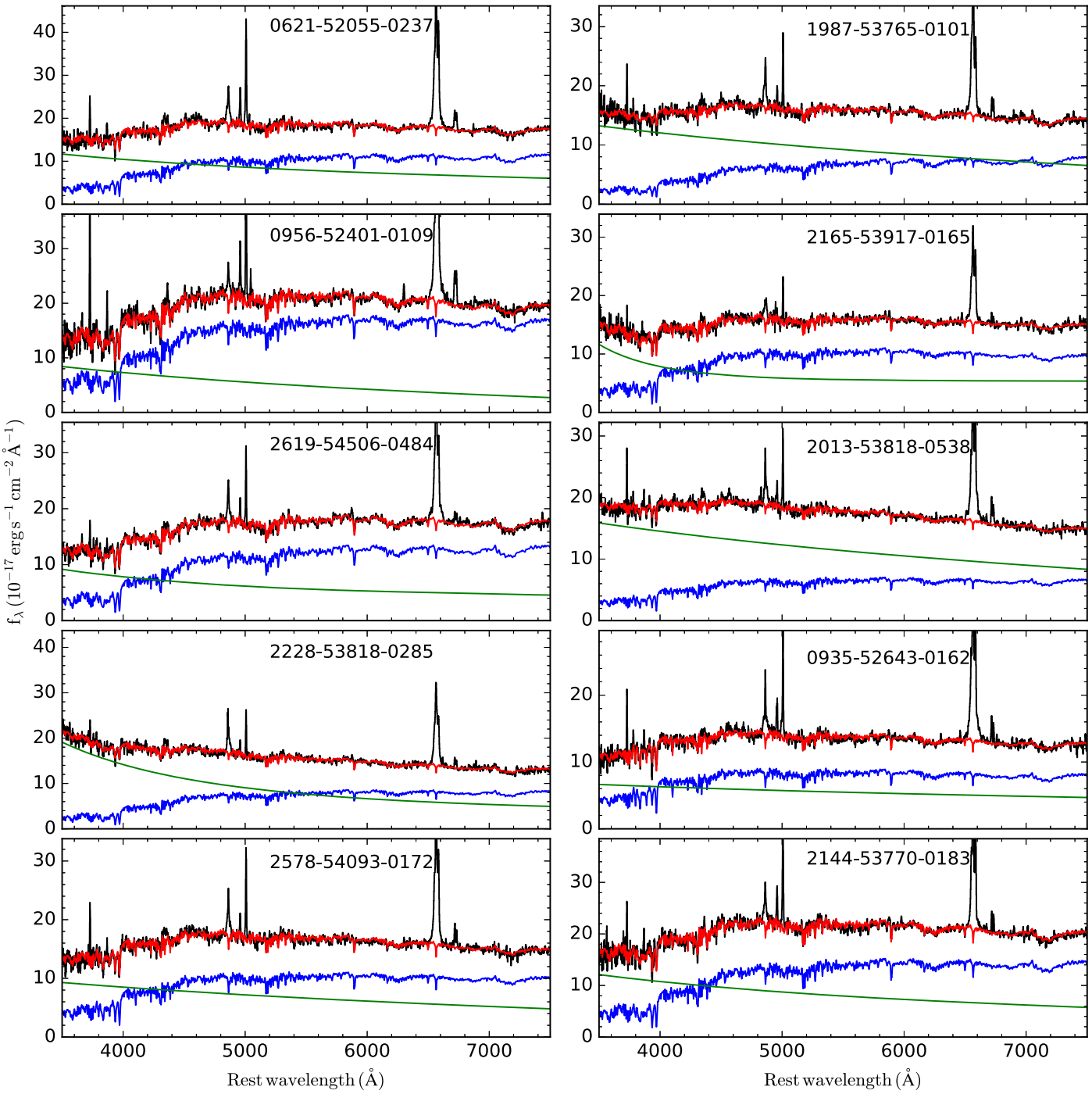

Figure 1. Subtraction of stellar contribution from spectra. Here, the black line shows the observed spectrum, the red line shows the best-fitted results, the green line shows power-law continuum fit and the blue line shows the stellar contribution. The labels indicate corresponding PLATE-MJD-FIBER of SDSS. The observed spectra were smoothed by a boxcar of 5 pixels only for illustration.

component around Hβ and Hα regions along with recent high-quality Fe II template spectra taken from Kovačević et al. (2010). In the Hβ region, with a wavelength range of 4385–5500 Å, apart from Hβ (having both narrow and broad components) the lines fitted are He IIλ4687 Å and [O III] λ 4959, 5007 Å doublet (with two Gaussian functions). In the Hα region, with a wavelength range 6280–6750 Å, the lines used in the fitting process are the narrow [O I]λ6300, 6363 Å, narrow [N II]λ6548, 6583 Å doublet, and the narrow [S II] λ6716, 6731 Å doublet along with Hα. Each of the narrow components are fitted with a single Gaussian having a maximum FWHM of 1200 km s^{-1}, following Shen et al. (2011). From theoretical arguments, Goad et al. (2012) suggest that the Balmer lines of NLSy1 galaxies are expected to have Lorentzian profile caused by the microscopic turbulence velocity of BLR clouds enhancing the line wings relative to the core, especially at a large radius. Observationally, it has also been noticed that the observed broad Balmer lines are best

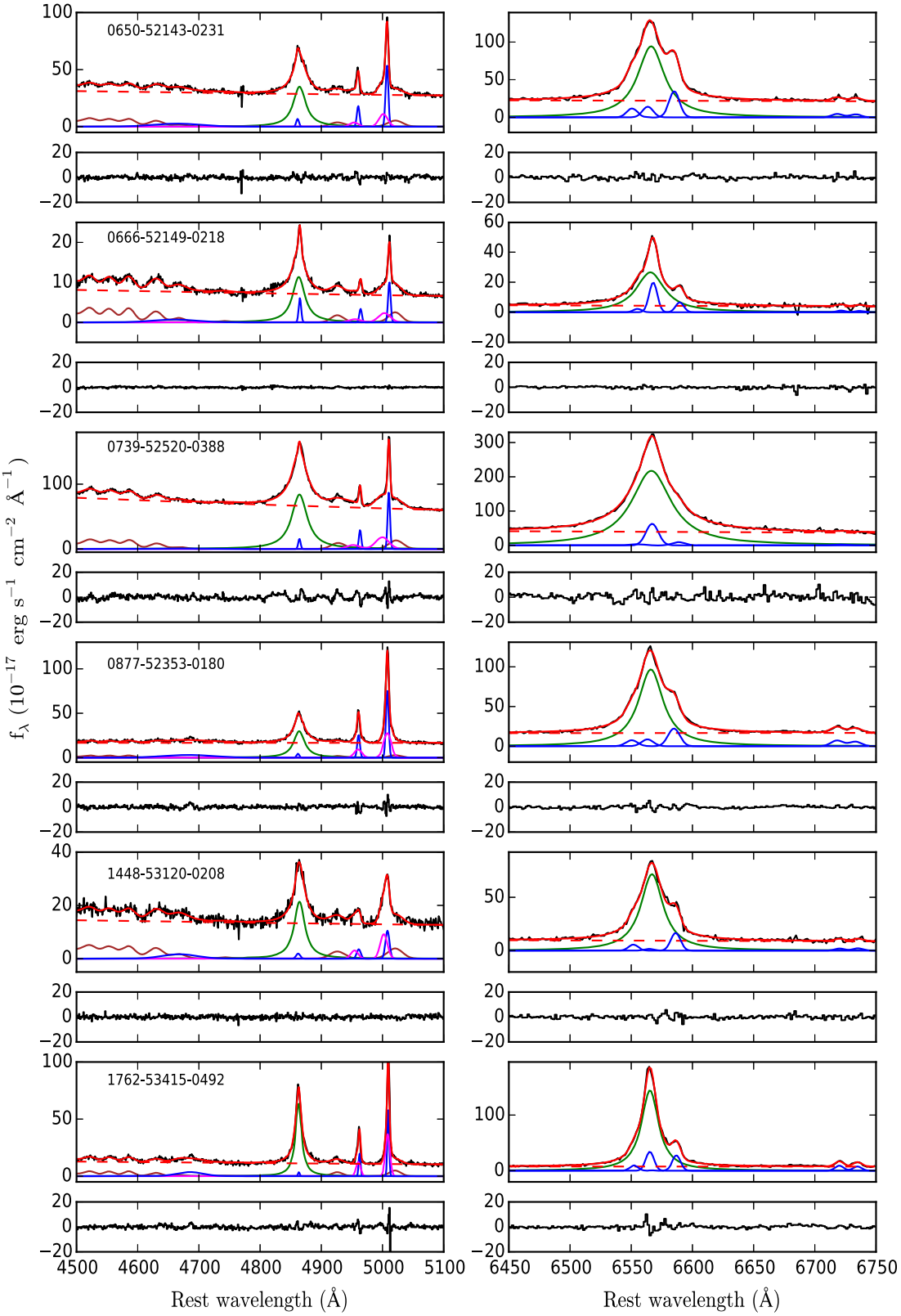

Figure 2. Examples of our simultaneous spectral fitting around Hβ (left) and Hα (right) emission line regions. The labels are PLATE-MJD-FIBER of SDSS. In each panel, the best-fitting results are shown in the top and the corresponding residual plots (horizontal black line) are shown below. In the Hβ region (left), the observed spectrum (black) and the overall fitted spectrum (red) are shown with the decomposed individual components; broad Hβ in green, narrow components (Hβ_n, [O III] doublet) and broad He II line in blue, broad [O III] doublet in magenta, and Fe II lines in brown. In the Hα region (right), the observed spectrum (black) and the overall fitted spectrum (red) is shown with the decomposed individual components; broad Hα in green and narrow components (Hα_n, [N II], [S II] doublets) in blue. Note that the x-scales of the figures are limited for the purpose of visualization.

Table 1
Emission Line Properties of NLSy1 Galaxies

ID	R.A.	Decl.	z	$\log(\lambda L_{\lambda})$	F(Hβ^{b})	FWHM (Hβ^{bc})	F(Hβ^{nc})	F([O III]^{tot})	FWHM([O III]^{nc})	F(Hα^{bc})	FWHM (Hα^{bc})	R_{4570}
(1)	(2)	(3)	(4)	(5)	(6)	(7)	(8)	(9)	(10)	(11)	(12)	(13)
1237-52762-0152	153.82315	8.56158	0.2439	43.00	70 ± 16	1153 ± 215	0 ± 0	30 ± 3	422 ± 0	456 ± 40	1623 ± 112	0.08
2341-53738-0008	148.35292	23.75970	0.2375	43.74	147 ± 9	2092 ± 124	13 ± 5	58 ± 30	495 ± 93	645 ± 12	2059 ± 34	0.80
0404-51812-0255	30.78837	−0.82019	0.5538	44.32	540 ± 21	2157 ± 72	0 ± 0	73 ± 5	624 ± 0	...	...	0.36
0710-52203-0270	46.41772	−0.37211	0.1894	42.63	48 ± 7	1510 ± 264	6 ± 3	32 ± 7	204 ± 43	117 ± 13	1478 ± 164	0.07
4567-55589-0768	152.25979	38.74255	0.7141	43.47	42 ± 9	2174 ± 405	1 ± 1	9 ± 6	218 ± 0	...	...	0.60
0401-51788-0475	25.29069	0.10748	0.4901	44.16	267 ± 25	1971 ± 132	37 ± 9	61 ± 24	949 ± 0	...	...	0.60
4546-55835-0798	14.16247	8.54443	0.5295	43.73	90 ± 12	2003 ± 210	5 ± 2	20 ± 2	465 ± 0	...	...	0.38
7448-56739-0145	144.59763	50.89967	0.6946	43.86	37 ± 6	1324 ± 178	0 ± 0	23 ± 4	943 ± 0	...	...	0.94
2229-53823-0306	181.80626	27.36376	0.2149	43.53	221 ± 13	468 ± 23	0 ± 0	87 ± 17	323 ± 0	778 ± 47	871 ± 36	0.75
7384-56715-0868	153.88019	46.90631	0.4754	43.43	41 ± 9	1925 ± 339	2 ± 1	17 ± 4	368 ± 0	...	...	0.83

Note. Columns are listed as follows: (1) SDSS ID (plate-mjd-fiber); (2) R.A. in degrees; (3) Decl. in degrees; (4) Redshift; (5) Logarithmic nuclear monochromatic luminosity at 5100 Å (erg s^{-1}); (6) Hβ broad component flux (10^{-17} erg s^{-1} cm^{-2}); (7) Hβ broad component FWHM (km s^{-1}); (8) Hβ narrow component flux (10^{-17} erg s^{-1} cm^{-2}); (9) Total (Broad+Narrow) [O III]λ5007 Å flux (10^{-17} erg s^{-1} cm^{-2}); (10) [O III] λ5007 Å narrow component FWHM (km s^{-1}); (11) Hα broad component flux (10^{-17} erg s^{-1} cm^{-2}); (12) Hα broad component FWHM (km s^{-1}); (13) Optical Fe II strength relative to Hβ broad component. The line fluxes are in the observed frame.

(This table is available in its entirety in machine-readable form.)

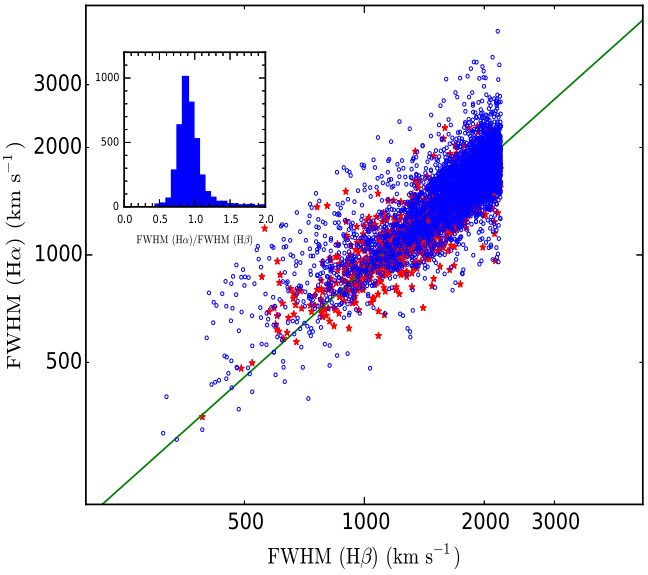

Figure 3. Correlation between FWHM of Hα and Hβ of 4021 NLSy1 galaxies in which both Hα and Hβ lines have been detected in our sample (circle) and the 1220 NLSy1 of ZH06 sample (star). The solid green line shows the best linear fit FWHM(Hα) = (0.909 ± 0.002) × FWHM(Hβ). The inset shows the histogram of the FWHM ratio of Hα to Hβ.

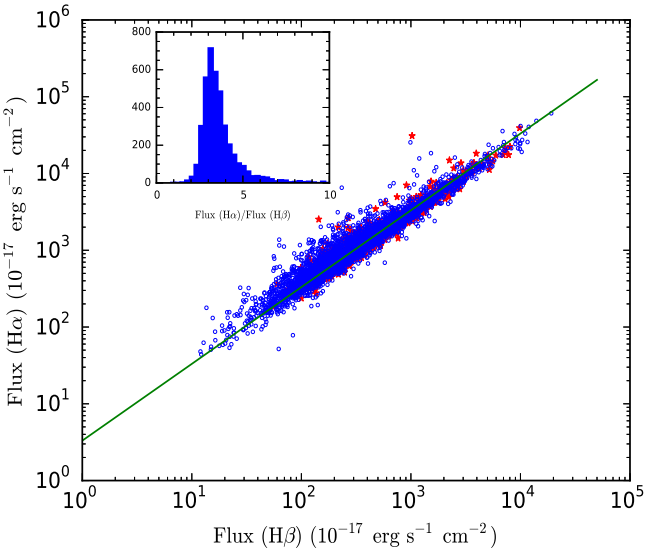

Figure 4. Correlation between the flux of Hα and Hβ of all the NLSy1 galaxies shown in Figure 3. The solid line shows the best linear fit F(Hα) = (3.049 ± 0.012) × F(Hβ). The inset shows the histogram of the flux ratio of Hα to Hβ.

characterized by a Lorentzian than a Gaussian profile (Moran et al. 1996; Véron-Cetty et al. 2001; Sulentic et al. 2002; Cracco et al. 2016).

In our fitting process, when both Hβ and Hα regions are fitted simultaneously, we allow a single Gaussian and Lorentzian functions for fitting both the broad Balmer components, where the algorithm automatically chooses among these functions the best-fitted function, which gives a similar width for both broad components of Balmer lines, Hβ and Hα. We also find that, in our fitting, the Lorentzian function is preferred compared to the Gaussian function, confirming the earlier claims by various authors as discussed above. This led us to choose a single Lorentzian function to model the broad component of Hβ when only the Hβ region was fitted. Note that if the narrow Hβ/Hα component is not required with the broad component, our iterative fitting procedure automatically drops it during minimization.

Spectral coverage of SDSS and BOSS allows us to carry out a simultaneous fitting of both Hα and Hβ regions for $z < 0.3629$, and for higher z (up to 0.8) only fitting of Hβ region was performed. During the fitting, the flux ratios of [O III] and [N II] doublets were fixed to their theoretical values, i.e., $F(5007)/F(4959) = 3$ and $F(6585)/F(6549) = 3$. Widths of all the narrow components in the Hβ region were tied with the narrow [O III] line width and the redshift of each doublet was tied together (see Shen et al. 2011). Similarly, in the Hα region, widths of all the narrow components were tied together with narrow [N II]λ6583 Å. A final fitting was carried out by simultaneously varying all the free parameters using Levenberg–Marquardt least-squares minimization, allowing us to estimate all emission line parameters including Fe II parameters along with the nuclear continuum contribution. Figure 2 shows few examples of emission line fitting around Hβ (left) and Hα (right). The corresponding residual plots are shown in the lower panels.

3. Criteria to Select NLSy1 Galaxies

Using the spectral fitting procedure described above, line parameters for all the 68,859 sources were estimated that were then used to find genuine NLSy1 galaxies provided they fulfill all of the following four criteria (Osterbrock & Pogge 1985; Goodrich 1989; Zhou et al. 2006).

1. The line flux of the broad component of Hβ[6] line is detected at more than a 3σ level.
2. The width of the broad Hβ component is greater than the width of the narrow forbidden line.
3. The FWHM of the broad Hβ emission line is narrower than 2200 km s^{-1}.
4. The flux ratio of total [O III] to total Hβ < 3, where total refers to the sum of both broad and narrow components flux.

Adopting the above criteria lead to the identification of 11,222 NLSy1 galaxies. All the fitting results were visually inspected and 217 appears to have large scatter in FWHM(Hβ)/FWHM (Hα) than others, mainly due to low S/N spectra. Those 217 spectra were fitted again using an additional constraint, FWHM (Hα) = 0.9 × FWHM(Hβ), which is the relation obtained by Zhang & Feng (2016). After the second fit, out of these 217 objects, 96 satisfy the condition of NLSy1 galaxies making a final sample of 11,101 NLSy1 galaxies. The details of the final list of sources are given in Table 1.

We note that the line width cutoff considered here is H$\beta \leqslant$ 2200 km s^{-1}, instead of the original value of H$\beta <$ 2000 km s^{-1} put by Goodrich (1989). This criterion was taken following ZH06 and considering the fact that the line width distribution of broad Balmer lines does not show any sharp cutoff between BLSy1 and NLSy1 population and rather shows a smooth distribution of width. Out of the 11,101 NLSy1 galaxies, 8577 have FWHM(Hβ) < 2000 km s^{-1}. For a majority of the sources in our sample, the Balmer lines were best-fitted with a Lorentzian than a Gaussian profile. This

[6] Hereafter, the line flux and width are of the broad component, unless stated otherwise.

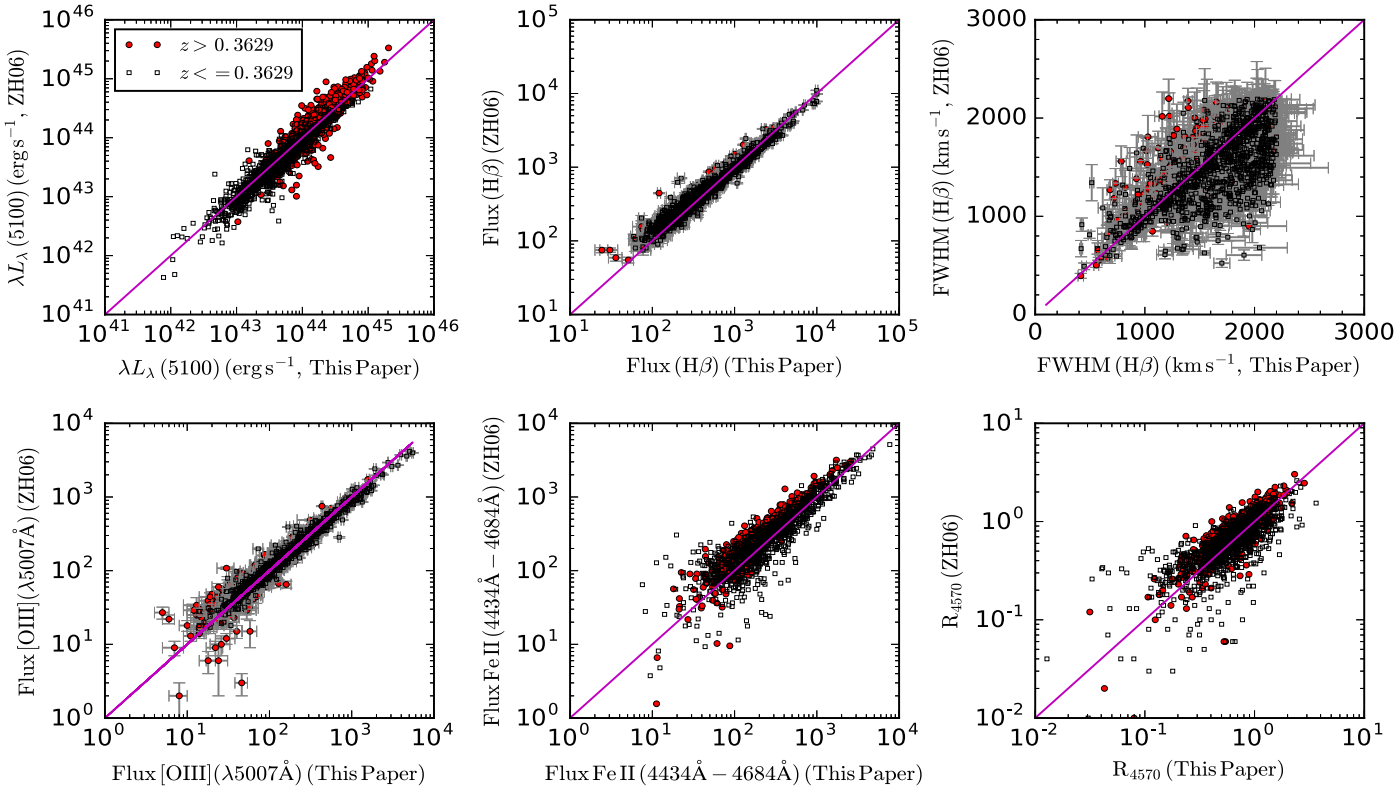

Figure 5. Comparison of our measurements with respect to ZH06 for nuclear monochromatic luminosity (upper left), broad Hβ line flux (upper middle), broad Hβ FWHM (upper right), flux of [O III]λ5007 Å (lower left), flux of Fe II (4434–4684 Å; lower middle), and strength of Fe II (lower right). The flux values are in units of 10^{-17} erg s^{-1} cm^{-2}.

reaffirms the claim made in the literature, as discussed in Section 2.2, that the broad Balmer lines of NLSy1 galaxy can be best-fitted by a single Lorentzian.

We have plotted in Figure 3, the FWHM of broad Balmer components for 4021 NLSy1 galaxies (dots) having $z < 0.3629$, so that both the Balmer lines are in the SDSS wavelength coverage. The stars in the figure indicate all of the 1220 NLSy1 galaxies from the ZH06 sample for comparison. We found FWHM (Hα) = (0.909 ± 0.002) × FWHM(Hβ). The inset plot shows the distribution of the FWHM ratio of Hα to Hβ. Similarly, we show in Figure 4, the flux of Hα broad component plotted against the flux of the broad component of Hβ. A linear least-squares fit gives us $F(\mathrm{H}\alpha) = (3.049 \pm 0.012) \times F(\mathrm{H}\beta)$. These values are consistent with those existing in the literature (e.g., see, ZH06 and Zhang & Feng 2016).

3.1. Comparison with the NLSy1 Galaxies Catalog of ZH06

Using the fitting procedure outlined above, we have arrived at a new sample of NLSy1 galaxies. For a consistency check, it will also be useful to test whether in our procedure we are able to retrieve the sample of NLSy1 galaxies reported by ZH06 using SDSS DR3. For that, we compared our sample with that of ZH06. We found that 1815 out of the 2011 sources reported by ZH06 are included in our sample. Our fitting procedure is thus able to recover 90% of the sources found by ZH06. The 10% of sources that are in the ZH06 sample but missed in our catalog might be due to (1) the fact that our selection considered the width of H$\beta \leqslant 2200$ km s^{-1}, whereas ZH06 considered either of the two Balmer lines[7] to have

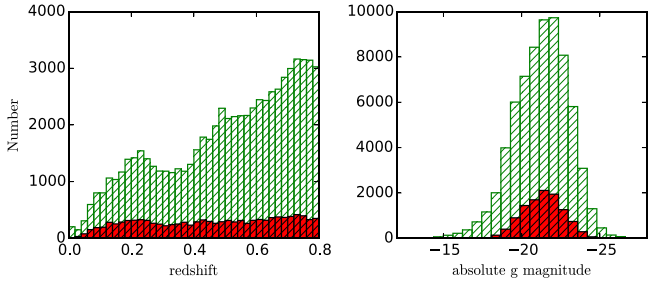

Figure 6. Distribution of redshift (left) and absolute g magnitude (right) of the parent sample of BLAGN (empty-hatched) and NLSy1 galaxies (filled).

FWHM $\leqslant 2200$ km s^{-1} and (2) that the ZH06 sample has 29 NLSy1 classified as "galaxy" in SDSS DR3, which are not included in our parent catalog of 114,806 candidates as our selection only considers the sources classified as "QSO" by SDSS pipeline. For those sources that are common to ours and the ZH06 sample, we found that typical errors in the FWHM of the Hβ broad component are around 5%, which is similar to the value of 6% quoted by ZH06. However, considering our whole sample of 11,101 sources, the median error in the FWHM of the Hβ broad component is around 7%.

In Figure 5, we compare our measurements with the values obtained by ZH06 for all the objects that are included in both of the catalogs. The nuclear monochromatic luminosity[8] (upper left), broad Hβ line flux (upper middle), broad Hβ FWHM (upper right), flux of [O III]λ 5007 Å (lower left), flux of Fe II

[7] Some objects do not have detectable Hβ but have Hα and thus included in the sample of ZH06.

[8] Only objects having nuclear light fraction (FC) > 0.25 in ZH06 have been plotted since the authors noted FC $\leqslant$ 0.25 is unreliable.

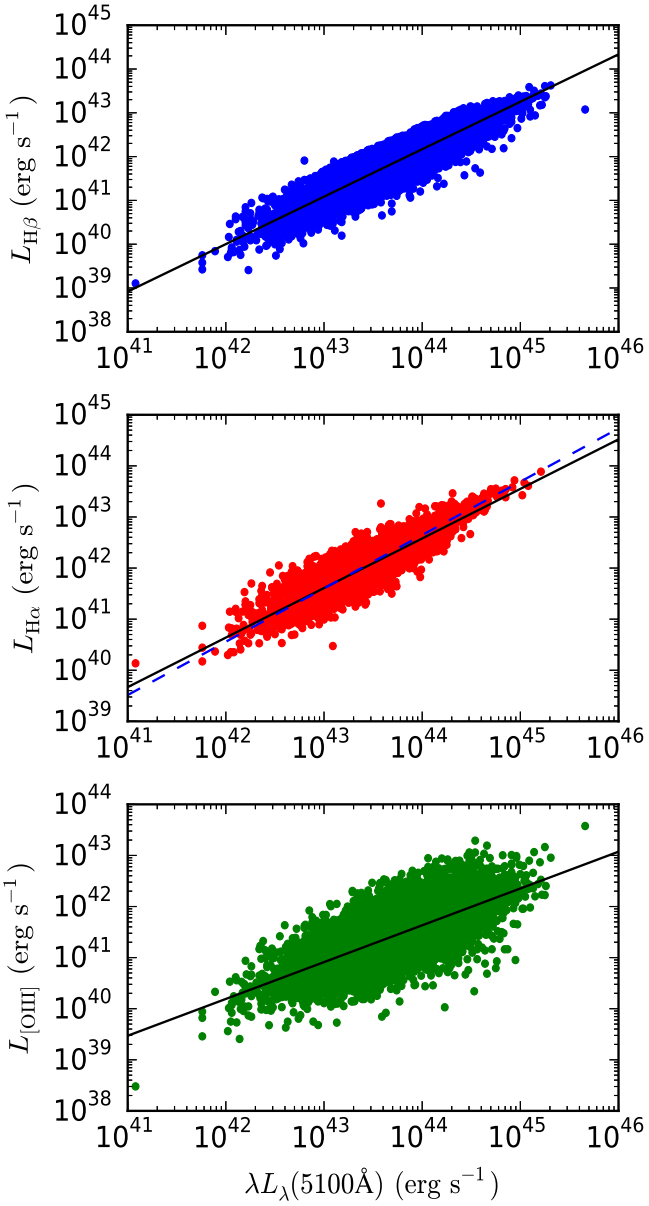

Figure 7. Correlations of the luminosity of Hβ (top), Hα (middle), and [O III] λ5007 Å (bottom) with monochromatic luminosity at 5100 Å. The best linear fit (solid line) is shown in each panel. The dashed line in the middle panel shows the relation of Jun et al. (2015).

(4434–4684 Å; lower middle), and strength of Fe II i.e., R_{4570} (lower right), defined as the ratio of Fe II flux in the wavelength range 4434 Å–4684 Å to the Hβ broad component flux, are shown in the plot. The circles represent objects having $z > 0.3629$, i.e., for the objects in which only the Hβ region is fitted while the empty squares are objects having $z < 0.3629$ in which both Hβ and Hα regions are fitted simultaneously. Our estimated λL_λ(5100 Å) closely matches with the measurements of ZH06. The logarithmic ratio of these two measurements has an average of 0.02 ± 0.17. Similarly, close matches between measurements of Hβ and [O III] line flux have also been found with the logarithmic ratio distribution having an average of -0.04 ± 0.08 and -0.02 ± 0.10 respectively. The Fe II flux and its strength are found to be similar to those of ZH06. The logarithmic ratio between our measurements to

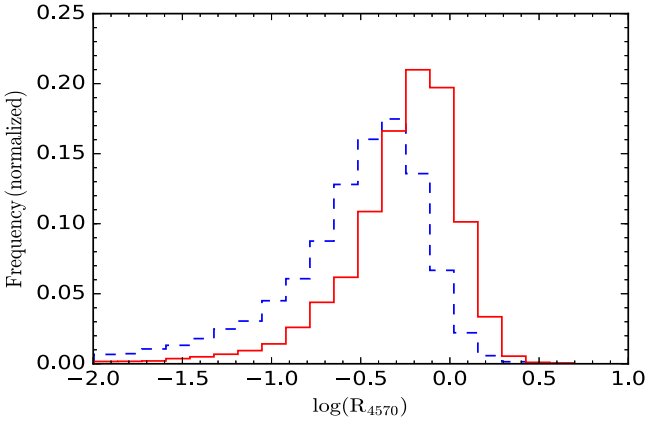

Figure 8. Distribution of the relative strength (R_{4570}) of Fe II emission with respect to Hβ for the NLSy1 sample (solid line) and BLSy1 sample (dashed line).

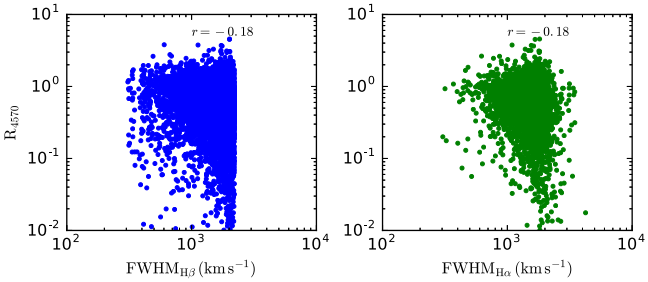

Figure 9. Correlation R_{4570} with FWHM of Hβ (left) and Hα (right). The Spearman correlation coefficient (r) is noted in each panel.

that of ZH06 has an average of -0.07 ± 0.19 and -0.03 ± 0.17 for Fe II flux and R_{4570} respectively. The close correspondence between various physical quantities (shown in Figure 5) deduced from the fitting process outlined here with those reported by ZH06 for sources that are common to the two studies, indicates the robustness of the fitting procedure adopted in this work.

The width of the Hβ broad emission line we measured also closely matches the measurement of ZH06. The ratio of these two measurements has a mean of 1.08 with a dispersion of 0.22. From the figure, it is evident that the Hβ widths of some objects having $z < 0.3629$, represented by empty square symbols, are overestimated in this work compare to ZH06 and deviate from the unit ratio line in some cases. This might be due to the differences in the fitting procedure adopted in this work and that used by ZH06. This overestimation of the FWHM of Hβ broad component for some objects by us could lead to some genuine NLSy1 galaxies being missed out, however, it would definitely prevent non-NLSy1 galaxies from being included in the sample. Also, our ability to retrieve 90% of the sources found by ZH06 reiterates the fact that our fitting procedure is robust, despite the minor difference in the methodology adopted in this work and that used in ZH06.

4. Properties of NLSy1 Galaxies of Our Catalog

The present sample increases the number of known NLSy1 galaxies by a factor of about five. It would therefore be of interest to investigate the ensemble properties of this new sample. Such an analysis using this large sample is indeed necessary to either confirm or refute the various properties of

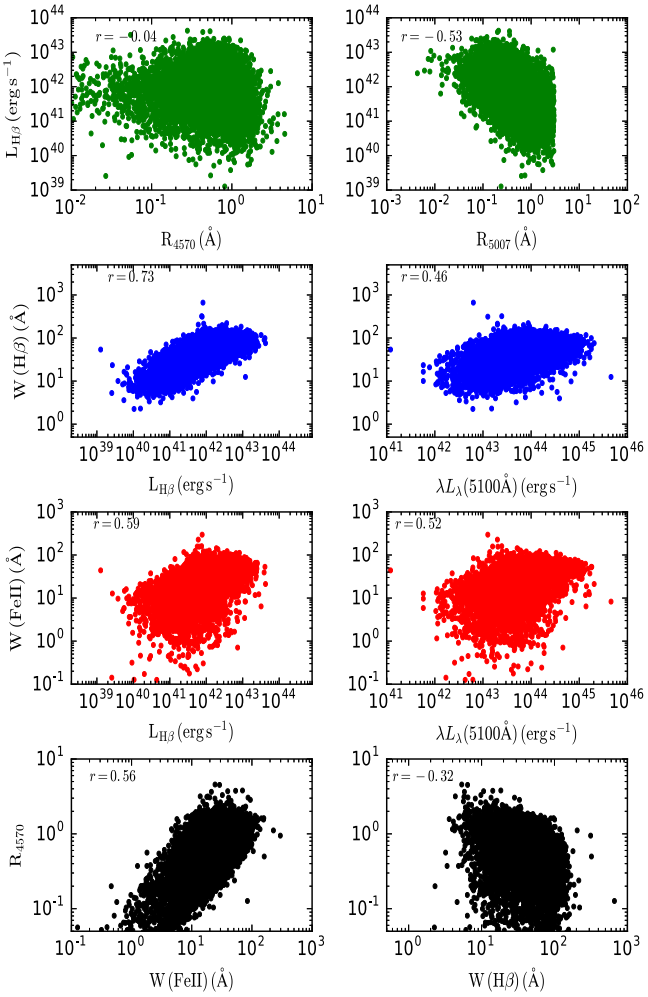

Figure 10. First panel: correlations of Hβ luminosity with relative Fe II strength, R_{4570}, (left) and the flux ratio of [O III] (λ5007 Å) to the total Hβ, R_{5007} (right). The objects with $R_{4570} > 0.01$ are only shown in the left panel and used to estimate the correlation of $L_{H\beta}$–R_{4570}. The cut on the right panel is due to $R_{5007} < 3$ used to select NLSy1. Second panel: correlation of Hβ equivalent width with the luminosity of Hβ (left) and monochromatic luminosity at 5100 Å (right). Third panel: correlation of Fe II equivalent width with the luminosity of Hβ (left) and monochromatic luminosity at 5100 Å (right). Fourth panel: the correlation of R_{4570} with the equivalent width of Fe II (left) and Hβ (right). The Spearman correlation coefficient (r) is noted in each panel.

NLSy1 galaxies that are based on a rather smaller sample size. We, therefore, present below some general characteristics of this new sample and make comparisons as and where needed. Detailed investigation of other physical properties of this sample will be presented elsewhere.

4.1. Redshift and Absolute Magnitude

The number of SDSS sources identified as "QSO" by the SDSS pipeline with $z < 0.8$ and a median S/N > 2 pixel^{-1} in SDSS DR12 is 68,859. From this initial set of sources, the number of NLSy1 galaxies selected based on our criteria is 11,101, which is about 16% of our original sample of broad-line AGNs. This is consistent with what is found earlier by Osterbrock (1988), Véron-Cetty et al. (2001), and ZH06. The redshift distribution and absolute g-band magnitude of all the BLAGN (parent sample: empty-hatched) and NLSy1 galaxy sample (filled region) are shown in Figure 6. The number of BLAGN increases with redshift in our parent sample, though the NLSy1 galaxies seem to be equally populated throughout $z < 0.8$. On the other hand, the absolute g-band magnitude distribution of both BLAGN and NLSy1 galaxies peaks at $M_g \sim -22$ mag. A similar peak in the absolute magnitude distribution is also noted by ZH06.

4.2. Luminosity, Equivalent Width, and Fe II Strength

Greene & Ho (2005) found a strong correlation between the luminosity of Balmer lines and optical continuum luminosity. Interestingly, such relations are valid over a wide range of luminosity ($10^{42} < L_{5100} < 10^{47}$ erg s^{-1}) and redshift ($0 < z < 6$), suggesting that the response of the BLR to the incident continuum is consistent across all redshifts and luminosities, i.e., the physical mechanism governing the correlation is the same in all AGNs (Jun et al. 2015). We estimated the luminosity of Hβ and Hα for all the objects in our sample having $0 < z < 0.8$ and $0 < z < 0.3629$ respectively. The correlation of monochromatic luminosity at 5100 Å with the luminosity of Hβ (top), Hα (middle), and [O III] λ5007 Å (bottom) is shown in Figure 7. All correlations are very strong, as found earlier by various authors (e.g., Greene & Ho 2005; Zhou et al. 2006; Jun et al. 2015). Linear least-squares fit yields

$$\log(L_{H\beta}) = (-5.53 \pm 0.21) + (1.084 \pm 0.004) \times \log(\lambda L_\lambda(5100\ \text{Å})). \quad (2)$$

$$\log(L_{H\alpha}) = (-0.17 \pm 0.34) + (0.971 \pm 0.007) \times \log(\lambda L_\lambda(5100\ \text{Å})). \quad (3)$$

$$\log(L_{[O\ III]}) = (9.87 \pm 0.29) + (0.721 \pm 0.006) \times \log(\lambda L_\lambda(5100\ \text{Å})). \quad (4)$$

The dashed line in the middle panel of Figure 7 represents the relation found by Jun et al. (2015), where they studied an $L_{H\alpha}$–L_{5100} relationship over a wide range of luminosity and redshift ($0 < z < 6$). The strong correlations between Balmer line luminosity and continuum luminosity over a wide range of luminosity and redshift suggest that the former can be used in measuring black hole mass when the latter is subjected to large uncertainty, especially in some AGNs, where the host galaxy contamination or emission from the jet is significant and optical continuum luminosity is difficult to estimate (e.g., Greene & Ho 2005). The relation of [O III] luminosity and continuum luminosity is particularly useful to measure intrinsic luminosity and the black hole mass of narrow emission line AGNs based on [O III] luminosity (e.g., Zakamska et al. 2003).

One of the main characteristics of NLSy1 galaxies is that they have strong Fe II emission (Vanden Berk et al. 2001; Zhou et al. 2006). The value of Fe II strength (R_{4570}) in a typical AGN is ~0.4 (see, Bergeron & Kunth 1984 and the reference therein) and about 0.8 in NLSy1 galaxies, as reported by ZH06. Our original sample provides us with a list of BLSy1 galaxies (FWHM$_{H\beta} > 2200$ km s^{-1}), allowing us to compare the Fe II strengths between NLSy1 and BLSy1 galaxies. The distributions of R_{4570} for both the samples are shown in Figure 8. The distribution for NLSy1 galaxies (solid line) peaks at larger R_{4570} having a mean and 1σ dispersion of 0.64 and 0.40, respectively, compared to the BLSy1 galaxies (dashed line), which has a mean and 1σ dispersion of 0.38 and 0.34, respectively. The Kolmogorov–Smirnov (K-S) two-sample test rejects the null hypothesis with a p-value of $<1 \times 10^{-100}$ that

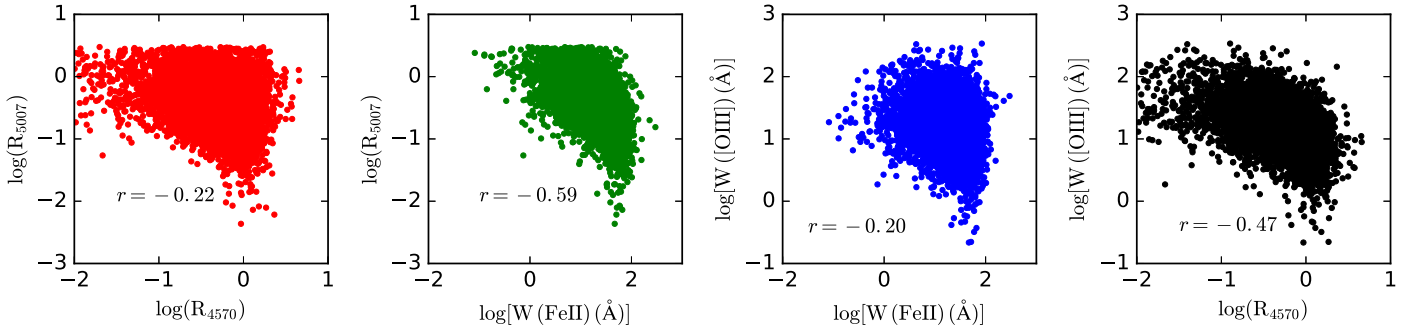

Figure 11. From left to right, the plots are R_{4570} vs. R_{5007}, R_{5007} vs. Fe II equivalent width (W), W([O III]) vs. W(Fe II), and W([O III]) vs. R_{4570}. The Spearman correlation coefficient (r) is noted in each panel. Only the objects with $R_{4570} > 0.01$ are considered for correlation analysis.

the two distributions are drawn from the same population. This is consistent with the earlier results in the literature (e.g., see, Vanden Berk et al. 2001; Zhou et al. 2006) and clearly indicates that NLSy1 galaxies are stronger Fe II emitters than BLSy1 galaxies. In our sample about 60% NLSy1 galaxies have $R_{4570} > 0.5$, about 16% show moderately strong Fe II emission with $R_{4570} > 1$, and about 0.5% show super strong Fe II emission ($R_{4570} > 2.0$; Lawrence et al. 1988). According to Gaskell (1985), the reason for having large R_{4570} in NLSy1 galaxies is due to their weak Hβ line instead of their strong Fe II emission.

In Figure 9, we plotted Fe II strength against the FWHM of broad Hβ (left) and Hα (right) of our sample. It is clear that there is a weak anti-correlation with the Spearman correlation coefficient of -0.18 in both cases (with a p-value of 1×10^{-21} and 1×10^{-29} respectively). This weak correlation in NLSy1 galaxies is consistent with the correlation found by ZH06. In Figure 10, we show the correlation between different derived parameters of our NLSy1 galaxy sample. No correlation is found between Hβ luminosity and R_{4570} (top left). We also calculated the equivalent widths (W) of Fe II and Hβ lines by the ratio of line flux to the continuum flux at 5100 Å i.e., $W = F_{\rm line}/F_c(\lambda = 5100$ Å). Interestingly, both W(Fe II) and W(Hβ) are found to be strongly correlated with the luminosity of Hβ line and monochromatic luminosity at 5100 Å (second and third panels). This is indeed similar to what was found by ZH06 and partially in agreement with Véron-Cetty et al. (2001) who found that the Hβ luminosity is not correlated with the equivalent width of Fe II but correlated with Hβ. The presence of such strong correlations suggest that NLSy1 galaxies are indeed a different class of objects compared to BLSy1 galaxies because the latter generally show no or very weak correlation. Moreover, a strong correlation between R_{4570} and W(Fe II) ($r = 0.5$), and an anti-correlation between R_{4570} with the equivalent width of Hβ has been found (fourth panel). This suggests that the observed large R_{4570} is not only due to weak Hβ but also due to strong Fe II, which is in agreement with Cracco et al. (2016) and partially in disagreement with Gaskell (1985). Also shown in Figure 10 is the correlation between Hβ luminosity against R_{5007}, which is the ratio of total [O III] flux to total Hβ (broad+narrow) flux ($R_{5007} = f\,[\text{O III}]^{\rm tot}/f\,(\text{H}\beta)^{\rm tot}$; the top-right corner). An anti-correlation is found that could be related to the weakness of Hβ in low-luminosity objects (middle-left panel) as found in Vanden Berk et al. (2001).

Objects with strong Fe II emission are found to have weak [O III] lines and vice versa (Grupe et al. 1999; McIntosh et al. 1999; Barrows et al. 2012); however, evidence of such anti-correlation has not been noted by Véron-Cetty et al. (2001). Several correlations of our NLSy1 galaxies are plotted in Figure 11. We find a weak anti-correlation between R_{5007} and R_{4570} (first panel, $r = -0.22$), a strong anti-correlation between R_{5007} and W(Fe II) (second panel, $r = -0.59$), a weak anti-correlation between W([O III]) and W(Fe II) (third panel, $r = -0.20$), and a moderately strong anti-correlation between W([O III]) and R_{4570} (fourth panel, $r = -0.47$). These observations thus confirm that Fe II strength is indeed stronger when [O III] is weak in NLSy1 galaxies.

4.3. Radio Properties

NLSy1 galaxies are generally radio quiet[9] with the radio loudness parameter $R < 10$. A fraction of about 7% of their population are known to be radio loud with $R > 10$, and a very small fraction of about 2.5% are found to be very radio loud with $R > 100$ (Komossa et al. 2006). The fraction of radio-loud NLSy1 galaxies is indeed small compared to the 15% we know in the quasar category of AGNs (Kellermann et al. 1989). However, the radio-loud quasar fraction is found to depend on redshift and luminosity and this fraction could be larger than 20% in low-redshift AGNs (Jiang et al. 2007). It is important to find more radio-loud NLSy1 galaxies, due to the discovery of γ-ray emission in half-a-dozen of them by *Fermi*, which argues for the presence of relativistic jets in these sources (e.g., see, Paliya et al. 2015). With an aim to find more radio-loud NLSy1 galaxies, we cross-correlated our sample with the FIRST survey (Catalog version 14dec17[10]) within a search radius of 2″. We find that about 555 sources (5%) are detected by FIRST.

In Figure 12, we show the distribution of logarithmic radio loudness (we define radio loudness as the ratio of 1.4 GHz flux to optical g-band flux, $R = F_{1.4\,\rm GHz}/F_{\rm g}$) in the upper panel, the distribution of radio power (middle panel), and the correlation between radio power and luminosity of [O III] (lower panel). The radio power ($P_{1.4}$) was estimated using $P_{1.4} = 4\pi D_L^2 (1+z)^{(\beta-1)} \nu_0 F_{\nu_0}$ (Cavagnolo et al. 2010), where ν_0 is the observed frequency of 1.4 GHz, D_L is the luminosity distance, and β is the radio spectral index taken to be 0.8 (Condon 1992). The $\log R$ distribution has a mean of 1.49 ± 0.82. Out of the 555 NLSy1 galaxies that are detected by FIRST, 177 are radio quiet ($R < 10$) and 378 are radio loud ($R > 10$). Their radio power ranges between $\log P_{1.4} = 37.6$ to 43.3 erg s^{-1} having a peak at about 40.5 erg s^{-1}. The distribution of $\log P_{1.4}$ has a mean of 40.0 ± 1.0 erg s^{-1}, which is

[9] The radio loudness parameter (R) is defined as the ratio of the radio flux density at 5 GHz to the optical flux density at 4400 Å (Kellermann et al. 1989).
[10] http://sundog.stsci.edu/first/catalogs.html

similar to the mean value of $\log P_{1.4}$ of 40.6 ± 1.1 erg s^{-1} found for the radio-detected BLSy1 galaxies in our sample indicating the influence of possible selection effects present in our sample of radio-detected sources. The 1.4 GHz radio power ($P_{1.4}$) is found to be correlated with the luminosity of [O III]. The Spearman correlation coefficient $r = 0.52$ with a p-value 1×10^{-41} confirms a strong positive correlation between these two parameters. A linear fit (solid line) yields

$$\log(P_{1.4}) = (0.976 \pm 0.06) \times \log(L_{[\mathrm{O\,III}]}) - (0.73 \pm 2.78). \quad (5)$$

This is similar to the correlation between radio power at 6 cm and luminosity of [O III] found by Greene & Ho (2007) for low-mass AGNs. However, dividing our radio-detected NLSy1 galaxies into different redshift ranges with bin size of 0.2, we found the correlation to vanish in all redshift bins except for $z < 0.2$.

4.4. X-Ray Properties

NLSy1 galaxies are known to show steep soft X-ray spectra and rapid X-ray variability. To find the X-ray counterparts to our sample, we cross-correlated our sample with the second *ROSAT* all-sky survey (2RXS) source catalog (Boller et al. 2016) within a search radius of 30″. This resulted in 1863 matches and amounts to 17% X-ray detection. The distribution of the soft X-ray (0.1–2 KeV) flux of all those NLSy1 galaxies is shown in Figure 13.

4.5. Electron Density of the Narrow Line Region

The most important density diagnostic of the NLR in AGNs is the intensity ratio of [S II]λ6716/λ6731 (Osterbrock 1989). There is ambiguity in the literature on the density of [S II] emission region in NLSy1 vis-a-vis BLSy1 galaxies. Using a sample of Seyfert 1 galaxies including seven NLSy1 galaxies, Rodríguez-Ardila et al. (2000) found that the typical density of the [S II] emission region in NLSy1 galaxies is lower than BLSy1 galaxies. According to Xu et al. (2007) BLSy1 galaxies avoid low-density ($n_e < 140$ cm^{-3}) while NLSy1 galaxies prefer low-density but show large dispersion in the density. Recently, Cracco et al. (2016) analyzed the electron density of BLSy1 and NLSy1 galaxies and found no difference in the electron-density distribution between the two classes. Because our sample of NLSy1 and BLSy1 galaxies are much larger than those used in earlier studies, we revisited the electron-density issue of NLR between NLSy1 and BLSy1 galaxies. For this, we estimated the intensity ratio of [S II]λ6716/λ6731 of 2551 NLSy1 and 5533 BLSy1 galaxies. To estimate electron density from this, the python code PyNeb[11] developed by Luridiana et al. (2015) was used. Using the PyNeb atomic data "IRAF_09," we calculated electron densities of the NLSy1 and BLSy1 galaxy sample for the intensity ratio of [S II]λ6716/λ6731 between 0.7 and 1.7 with a fixed temperature $T = 10^4$ K (see also Cracco et al. 2016). The above criteria provided us density estimates of 2020 NLSy1 and 4744 BLSy1 galaxies.

Figure 14 shows the variation of electron density against FWHM of Hβ for both NLSy1 (dots) and BLSy1 (stars) galaxies. The horizontal dashed line at $n_e = 140$ cm^{-3} (i.e., $\log n_e = 2.146$ cm^{-3}) separates the low- and high-density regions, whereas, the vertical dashed line at 2200 km s^{-1} separates the sources into BLSy1 and NLSy1 galaxies. Out of the 2020 NLSy1 galaxies, 509 (25%) have $\log n_e < 2.146$ cm^{-3} (zone A), while 1511 (75%) have $\log n_e > 2.146$ (zone B). In the case of BLSy1 galaxies (zone C), 725 out of 4744 objects (15%) have $\log n_e < 2.146$ and the remaining 4018 objects (85%) have $\log n_e > 2.146$ cm^{-3}. Our study suggests that about 15% of BLSy1 galaxies in our sample have $\log n_e < 2.146$ cm^{-3}, which

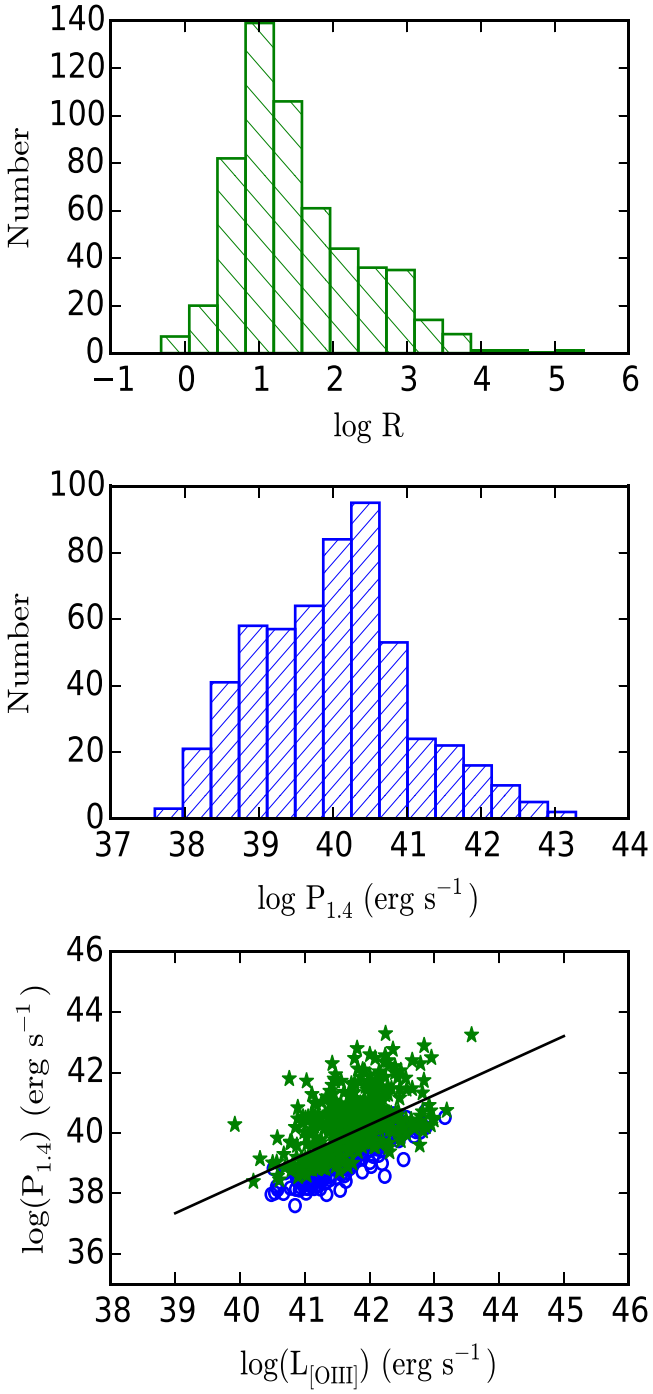

Figure 12. Distributions of logarithmic radio loudness ($\log R$, top) and radio power at 1.4 GHz (middle) of the NLSy1 in our sample. The correlation of radio power and [O III] (λ5007 Å) luminosity is shown at the bottom. Star symbols indicate NLSy1 with $\log R > 1$, while empty circles indicate NLSy1 with $\log R < 1$. The best linear fit of all radio-detected NLSy1 is shown by a solid black line.

[11] http://www.iac.es/proyecto/PyNeb/

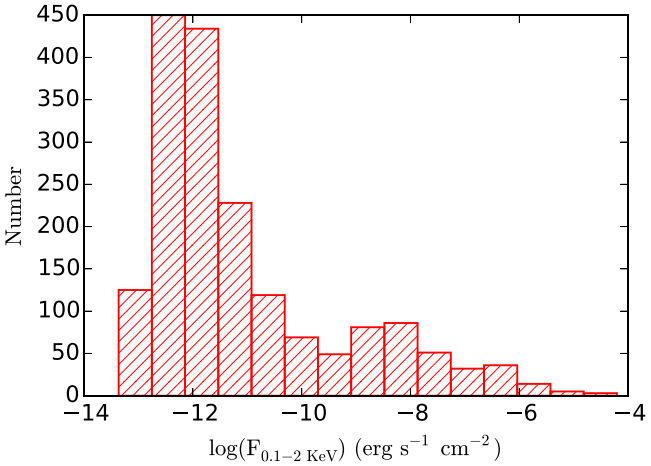

Figure 13. Distribution of soft X-ray flux of NLSy1 in our sample.

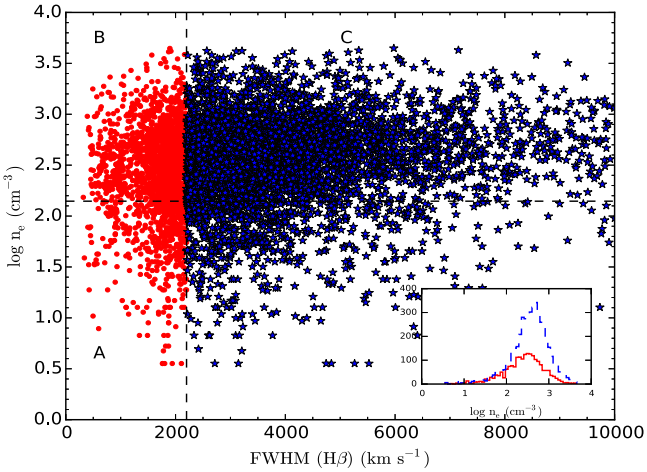

Figure 14. Relation between electron density and FWHM of Hβ. The dots and stars represent the density of NLSy1 and BLSy1 respectively. The dashed horizontal and vertical lines indicate density 140 cm^{-3} and the dividing line width (i.e., FWHM(Hβ) = 2200 km s^{-1}) between two samples respectively. The lower inset plot shows a density histogram for NLSy1 (solid line) and BLSy1 (dashed line).

is not in agreement with Xu et al. (2007) who found BLSy1 galaxies to have $\log n_e > 2.146$ cm^{-3}. This disagreement is likely due to the low number statistics of objects used by Xu et al. (2007) in their analysis. However, we find a weak trend of low-density NLR in NLSy1 and a high-density NLR in BLSy1 galaxies. In fact, a very weak but positive correlation between n_e and FWHM (Hβ) is found using the Spearman test of correlation having a correlation coefficient of $r = 0.12$, and a p-value of 1×10^{-23}, suggesting lower electron density in the NLR of NLSy1 galaxies than BLSy1 galaxies. The density distributions for NLSy1 (solid) and BLSy1 (dashed) galaxies is shown in the inset of Figure 14. We find mean $\log n_e$ values of 2.40 ± 0.47 cm^{-3} and 2.54 ± 0.44 cm^{-3} for NLSy1 and BLSy1 galaxies respectively. Applying the K-S statistic, we obtained $r = 0.148$ and p-value of 7×10^{-28} rejecting the null hypothesis that both the distributions are drawn from the same population.

4.6. Black Hole Mass and Eddington Ratio

The mass of the central super massive black hole of our sample of NLSy1 galaxies, as well as the BLSy1 galaxies, were estimated using the virial relation. Considering virial motion of BLR clouds, black hole mass ($M_{\rm BH}$) can be written as

$$M_{\rm BH} = f R_{\rm BLR} \Delta v^2 / G, \quad (6)$$

where Δv is the FWHM of broad emission line and $R_{\rm BLR}$ is the radius of the BLR (Wandel et al. 1999; Kaspi et al. 2000). The factor f known as scale factor depends strongly on the geometry and kinematics of the BLR (Rakshit et al. 2015). Considering the spherical distribution of clouds, we used $f = 3/4$ and estimated $R_{\rm BLR}$ from reverberation mapping scaling relation,

$$\log\left(\frac{R_{\rm BLR}}{\rm lt-day}\right) = K + \alpha \times \log\left(\frac{\lambda L_\lambda (5100\ \text{Å})}{10^{44}}\ \text{erg s}^{-1}\right), \quad (7)$$

where K (1.527) and α (0.533) are taken from Bentz et al. (2013) who carefully subtracted the host galaxy contribution to calibrate the relationship between BLR size and the monochromatic luminosity at 5100 Å. The Eddington ratios $\xi_{\rm Edd}$, defined as $L_{\rm bol}/L_{\rm Edd}$ were estimated considering $L_{\rm Edd} = 1.3 \times 10^{38} M_{\rm BH}/M_\odot$ erg s^{-1}. Following Kaspi et al. (2000), we

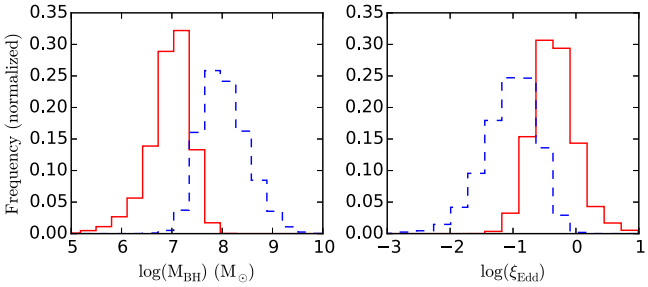

Figure 15. Distributions of black hole mass (left) and Eddington ratio (right). The NLSy1 is shown by a solid line while BLSy1 is shown by a dashed line. NLSy1 has a lower mass and higher Eddington ratio than BLSy1.

estimated $L_{\rm bol}$ assuming $L_{\rm bol} = 9 \times \lambda L_\lambda (5100\ \text{Å})$ erg s^{-1} (see also Xu et al. 2012).

The distribution of black hole mass is plotted in the left panel of Figure 15 for both NLSy1 (solid line) and BLSy1 (dashed line) galaxies. In the case of NLSy1 galaxies, the $\log(M_{\rm BH})$ distribution has a mean of 6.9 $M_\odot$ with a dispersion of 0.41 $M_\odot$, while in the case of BLSy1 galaxies, the $\log(M_{\rm BH})$ distribution has a mean of 8.0 $M_\odot$ with a dispersion of 0.46 $M_\odot$. A K-S test applied on the distributions points that both distributions are remarkably different having a K-S statistic value of 0.83 and a p-value of $<1 \times 10^{-150}$. NLSy1 galaxies thus have lower $M_{\rm BH}$ than BLSy1 galaxies. The right panel of Figure 15 shows the distribution of the Eddington ratio. The log ($\xi_{\rm Edd}$) distribution for the sample of NLSy1 and BLSy1 galaxies has mean values of -0.34 and -1.03 with standard deviations of 0.34 and 0.42 respectively. This suggests that NLSy1 galaxies have higher Eddington ratios than BLSy1 galaxies. A K-S test confirms the significant difference between the two Eddington ratio distributions with a K-S statistic of 0.64 and a p value $<1 \times 10^{-150}$. Thus, our results are in agreement with those available in the literature that NLSy1 galaxies have lower black hole mass and higher Eddington ratio than BLSy1 galaxies (e.g., Xu et al. 2012).

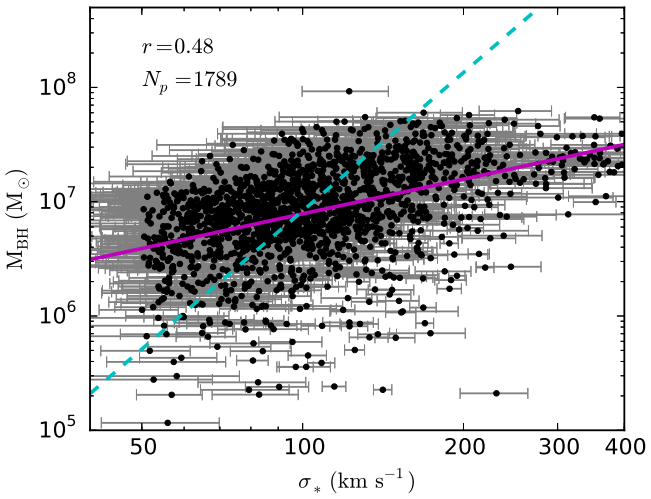

Figure 16. Correlation of black hole mass with host galaxy velocity dispersion σ_*. The dashed line shows the expected relation of Tremaine et al. (2002) and the solid line shows the best linear fit. The label N_p indicates the total number of NLSy1 galaxies used in the plot.

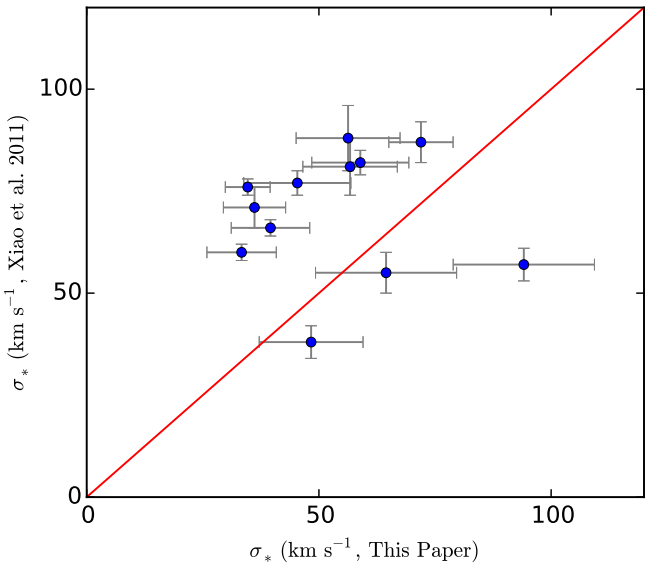

Figure 17. Values of σ_* as obtained in this paper is plotted along the x-axis and the values obtained by Xiao et al. (2011) is plotted along the y-axis. The unit ratio line is represented by a solid line.

4.7. $M_{\rm BH}$–σ_* Relation

To understand the evolution and growth of the black hole it is important to know the connections, if any, between $M_{\rm BH}$ and host galaxy properties. Available observational evidence points to a close correlation between $M_{\rm BH}$ and bulge mass (Kormendy & Richstone 1995; Magorrian et al. 1998) as well as $M_{\rm BH}$ and σ_* (Ferrarese & Merritt 2000; Gebhardt et al. 2000; Kormendy & Ho 2013; McConnell & Ma 2013), which suggests stellar velocity as a fundamental parameter of black hole evolution. Seyfert galaxies are also known to follow the same $M_{\rm BH}$–σ_* as that shown by the normal galaxy population (Nelson et al. 2004; Woo et al. 2010, 2013). Since NLSy1 galaxies have low-mass black holes, it is crucial to test the extension of the $M_{\rm BH}$–σ_* relation to the low-mass end of NLSy1 galaxies (Mathur et al. 2001), which is attempted here for our sample. For this, we considered only those sources for which the spectra have a median S/N $>$ 10 pixel^{-1}, and obtained σ_* for 1789 NLSy1 galaxies. The σ_* is the width (second-order moment) of the best-fitted Gaussian broadening function used in the convolution of our SSP template (see Equation (1)). In Figure 16, the top panel shows the variation of viral black hole mass against σ_*. The solid line is the best linear least-squares fit to the data. A moderately strong correlation is found between the two parameters with a Spearman rank correlation coefficient 0.48 and a p-value of 7×10^{-103}. Using the well-known $M_{\rm BH}$–σ_* relation for inactive galaxies as defined by Tremaine et al. (2002),

$$\log\left(\frac{M_{\rm BH}}{M_\odot}\right) = 8.13 + 4.02 \times \log\left(\frac{\sigma_*}{200\ {\rm km\ s^{-1}}}\right), \qquad (8)$$

we calculated the $M_{{\rm BH},\sigma_*}$ using σ_*. This relation is indicated by a dashed line in the figure. About 50% of the NLSy1 galaxies of our sample lie below the dashed line and $M_{\rm BH}$ values at the low-mass end have large error bars. This suggests that NLSy1 galaxies do not follow the $M_{\rm BH}$–σ_* relation of inactive galaxies. This closely follows the finding by ZH06, however, it is in contrast to that of Woo et al. (2015) who report the NLSy1 galaxies follow the $M_{\rm BH}$–σ_* relation of BLSy1 and inactive galaxies.

Xiao et al. (2011) presented accurate measurements of σ_* for 76 Seyfert 1 galaxies with low black hole mass using high-resolution spectra obtained from Keck Echellette Spectrograph and Imager and the *Magellan* Echellette (MagE). Out of these, 22 objects are present in our catalog. However, only for 12 objects, we have a σ_* measurement, non-zero at the 3σ level. The σ_* values of those objects are plotted in Figure 17. The solid line represents the unit ratio line. Note that the spectra of all these 12 objects are obtained by SDSS with a fiber diameter of 3″. The ratio of σ_* between our measurement and that of the Xiao et al. (2011) is 0.80 ± 0.35. The large scatter might be due to low resolution as well as poor S/N in the spectra. However, the figure indicates that our result largely follows the result of Xiao et al. (2011) indicating that SDSS spectra could be used to study σ_* for a large sample. However, to accurately estimate σ_* high-resolution spectra with good S/Ns is needed where detailed modeling of the host galaxy contribution can be carried out.

Measuring σ_* of high-redshift Seyfert galaxies is very difficult mainly because their cores outshine the host. However, the narrow component of the [O III] line was used as a surrogate of σ_*, though using it various authors reported conflicting results. Most of these studies found that NLSy1 galaxies fall below the relation than the BLSy1 galaxies (Mathur et al. 2001; Botte et al. 2004; Grupe & Mathur 2004). On the contrary, Wang & Lu (2001) and Wandel (2002) found that most of the NLSy1 galaxies fall on the line. The origin of such a conflicting result could be due to the asymmetry in [O III] line (Véron-Cetty et al. 2001; Cracco et al. 2016) because of which Wang & Lu (2001) used the width of [O III] line after subtracting the blue wings. A similar argument was also made by Komossa & Xu (2007), who found that the width of the [O III] line can be used only after subtracting blue wings and excluding the core component of [O III] lines with strong blueshifts.

To revisit the use of the width of the [O III] line as a surrogate of σ_*, we estimated the width of the narrow component of the [O III] line (FWHM$_{[{\rm OIII}]_{\rm n}}$) for all the NLSy1 galaxies, but use only those with a median S/N $>$ 10 pixel^{-1}

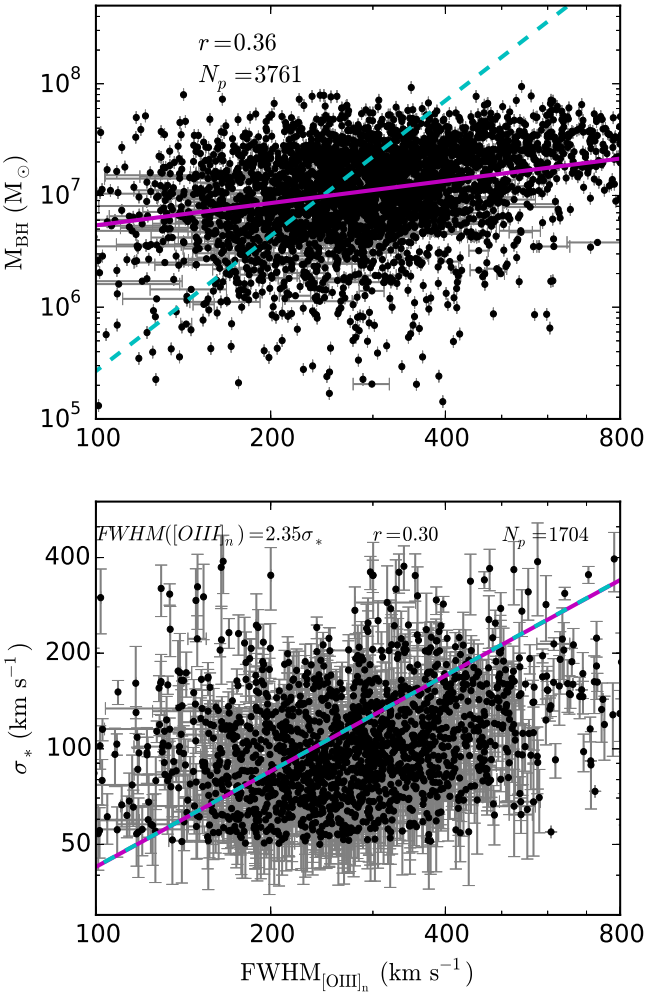

Figure 18. Top: correlation of black hole mass with FWHM([O III]$_n$). The dashed line shows the expected relation of Tremaine et al. (2002), considering $\sigma_* = \mathrm{FWHM([O\,III]_n)}/2.35$, and the solid line shows the best linear fit. Bottom: plot of σ_* against FWHM([O III]$_n$). The best linear fit to the relation is shown by a solid line having a slope $\mathrm{FWHM([O\,III]_n)} = 2.35\sigma_*$, which matches the dashed line of the FWHM = 2.35× standard deviation.

and a narrow component if [O III] is detected with more than 3σ. We further deconvolved the lines to remove the effect of SDSS spectral resolution and plotted $M_{\rm BH}$ against $\mathrm{FWHM_{[O\,III]_n}}$ in the upper panel of Figure 18. A correlation is indeed present though weak mainly due to large scatter in the latter. Furthermore, in the lower panel of Figure 18, we plotted σ_* against $\mathrm{FWHM_{[OIII]_n}}$. The best linear fit indicated by the solid line, $\mathrm{FWHM_{[OIII]_n}} = 2.35\sigma_*$, is superimposed on the dashed line of FWHM = 2.35× standard deviation. There is an indication that many of the objects are falling off the line but large scatter in the width prevents us from making any firm statement. However, the plot clearly indicates that $\mathrm{FWHM_{[O\,III]_n}}$ can be a proxy of σ_* as previously claimed and widely used in various literature as mentioned above.

4.8. Effect of Inclination

The reasons behind small $M_{\rm BH}$ and large Eddington ratios in NLSy1 galaxies is still unclear. The small Balmer line width that gives rise to small $M_{\rm BH}$ based on the virial relation could be due to geometrical effects. Increasing evidence suggests that NLSy1 galaxies can have $M_{\rm BH}$ and Eddington ratios

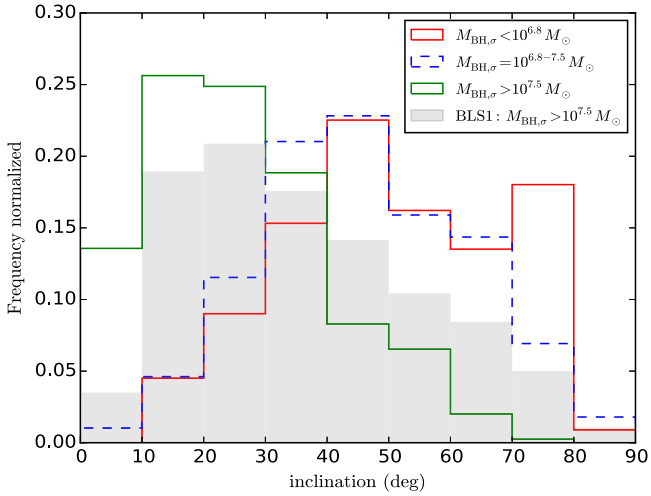

Figure 19. Distribution of inclination in degree for a range of $M_{\rm BH,\sigma_*}$. The shaded area represents the inclination distribution of BLSy1 having $M_{\rm BH,\sigma_*} > 10^{7.5}\,M_\odot$ and similar luminosity like NLSy1.

similar to BLSy1 galaxies. For example, a recent, spectro-polarimetric study of the radio-loud NLSy1 galaxy PKS 2004 −447 by Baldi et al. (2016) revealed that the width of the Hα line in the polarized spectrum is 9000 km s^{-1}, which is six times broader than the width seen in direct light, yielding a $M_{\rm BH}$ of $6 \times 10^8\,M_\odot$ and much higher than the $5 \times 10^6\,M_\odot$ estimated using the Hβ line seen in direct light. Also, Calderone et al. (2013), by modeling the optical and UV data for a sample of 23 radio-loud NLSy1 galaxies with a Shakura & Sunyaev disk, found $M_{\rm BH}$ larger than $10^8\,M_\odot$, about six times larger than those obtained from single epoch viral black hole mass estimates. Furthermore, Decarli et al. (2008) suggested that if the BLR has a disk-like geometry as opposed to a spherical geometry, the geometrical factor (f) can fully account for the observed mass deficit in NLSy1 galaxies and $\xi_{\rm Edd}$ turns out to be similar to BLSy1 galaxies (see also Liu et al. 2016).

Arguments in favor and against the face-on view of NLSy1 galaxies are available in the literature. Evidences in favor of the face-on view include small widths of the Balmer line due to projection effect (Osterbrock & Pogge 1985; Bian & Zhao 2004), anisotropic emission of Fe II (Marziani et al. 2001), and detection of γ-rays by *Fermi* Gamma-ray space telescope in about half a dozen of the radio-loud NLSy1 galaxies (Abdo et al. 2010). Evidence against the face-on view come from the study of polarization observations by Smith et al. (2005). Furthermore, studying a sample of radio-loud NLSy1 galaxies, Komossa et al. (2006) and Yuan et al. (2008) could not confirm the face-on view of NLSy1 galaxies. An estimate of the inclination angle (i) of NLSy1 galaxies can be obtained using

$$f = \frac{GM_{\rm BH,\sigma_*}}{R_{\rm BLR}\,\mathrm{FWHM}^2_{\rm H\beta}} = (\sin^2 i + \sin^2\omega)^{-1} \qquad (9)$$

where ω is the half-opening angle of BLR geometry, $\omega = 90°$ for a spherical geometry.

Considering a flat BLR ($\omega = 0$), we estimated i for all of the objects with $f > 1$. Figure 19 shows the distribution of inclination for different $M_{\rm BH,\sigma_*}$. The mean of the distributions are 26°, 46°, and 50° for $M_{\rm BH,\sigma_*} > 10^{7.5}\,M_\odot$, $M_{\rm BH,\sigma_*} = 10^{6.8-7.5}\,M_\odot$ and $M_{\rm BH,\sigma_*} < 10^{6.8}\,M_\odot$, respectively, though all distributions are have

large spreads in inclination. For the purpose of comparison, in the same way, we also calculated i for the BLSy1 galaxies with $M_{\mathrm{BH},\sigma_*} > 10^{7.5}\,M_\odot$ and similar luminosity like the NLSy1 galaxies. This distribution is plotted with shaded color. The average value in the case of BLSy1 galaxies is 41°, which is larger than the average inclination of NLSy1 galaxies with $M_{\mathrm{BH},\sigma_*} > 10^{7.5}\,M_\odot$. This result is consistent with Zhang & Wu (2002) who estimated an inclination angle of about 20 BLSy1 and 50 NLSy1 galaxies and found that the latter have systematically lower inclination angles than the former. Thus, the idea that the narrow width of the emission line in NLSy1 is due to the orientation effect seems to be true.

5. Summary

Large-scale surveys are the most effective ways to have a complete census of the different classes of AGNs. We have carried out a systematic search for new NLSy1 galaxies in SDSS DR12 by using a sample of 68,859 objects having $z < 0.8$ and a median of $\mathrm{S/N} > 2$ pixel^{-1}. For this, we have developed procedures to carefully subtract the host galaxy contribution, taking into account the Fe II emission and extracting the nuclear continuum contribution, and then fitting the emission lines to extract crucial emission line parameters. Applying our developed procedure to SDSS DR12 database, we compiled a new sample of NLSy1 galaxies. The major findings of this work are as follows.

1. Adopting the criteria of FWHM(Hβ) $\leqslant$ 2200 km s^{-1} and [O III]/H $\beta < 3$ to our derived emission line parameters of "QSO" sources in SDSS DR12, we arrived at a new sample of 11,101 NLSy1 galaxies. This is about five times larger than the 2011 NLSy1 galaxies known previously from SDSS DR3 (ZH06).
2. The broad Balmer component of the majority of the NLSy1 galaxies can be best-fitted with a Lorentzian than a Gaussian profile reaffirming the claim made in the literature with a smaller sample.
3. A total of 68,859 objects with $z < 0.8$ and a median of $\mathrm{S/N} > 2$ pixel^{-1} has been studied. Of this, 11,101 are NLSy1 galaxies, which indicate that ∼16% of AGNs are NLSy1 galaxies. The absolute magnitude of this sample peaks at around $M_g \simeq -22$ mag.
4. The monochromatic luminosity at 5100 Å is found to be strongly correlated with luminosity of Hβ, Hα, and [O III] lines, which is in agreement with the results already available in the literature (e.g., Greene & Ho 2005).
5. The strength of Fe II emission in NLSy1 galaxies is a factor of two larger than BLSy1 galaxies. The R_{4570} distribution peaks at 0.64 in NLSy1 galaxies and 0.38 in BLSy1 galaxies. About 0.5% of NLSy1 galaxies shows strong Fe II emission with $R_{4570} > 2$.
6. The equivalent width of Fe II and Hβ is found to be strongly correlated with the luminosity of Hβ and the monochromatic luminosity at 5100 Å, which agrees with ZH06 and partially with Véron-Cetty et al. (2001). An anti-correlation between $L_{\mathrm{H}\beta}$ with R_{5007} is found, however, no correlation with R_{4570} is present.
7. In our new sample of NLSy1 galaxies, 555 (5%) sources are detected in the FIRST survey. Such a low fraction of radio emitting NLSy1 galaxies (7%) is also reported by ZH06. Thus, NLSy1 galaxies do show the radio-loud/radio-quiet dichotomy seen in the quasar category of AGNs. The distribution of radio power distribution peaks at 40.5 erg s^{-1} and shows a strong correlation with [O III] luminosity at $z < 0.2$.
8. About 17% of our sample of NLSy1 galaxies are detected in the soft X-ray band by *ROSAT*. The soft X-ray flux distribution peaks at low flux, around 10^{-12} erg s^{-1} cm^{-2}, while the number falls rapidly for high flux.
9. The strong difference in M_{BH} (calculated using viral methods) and Eddington ratio are found between NLSy1 and BLSy1 galaxies. NLSy1 galaxies have low M_{BH} and high Eddington ratio compared to BLSy1 galaxies.
10. Electron density in the NLR of NLSy1 galaxies is found to be low and widely scattered compared to BLSy1 galaxies. About 25% of NLSy1 and 15% of BLSy1 galaxies have low density $n_e < 140$ cm^{-3}. This is against the finding of Xu et al. (2007) who found the BLSy1 galaxies not to have $n_e < 140$ cm^{-3}. Thus, the "zone of avoidance" in density found for BLSy1 galaxies by Xu et al. (2007) does not exist.
11. Stellar velocity dispersion (σ_*) has been obtained for 1789 NLSy1 galaxies. A positive correlation has been found between σ_* and M_{BH} and a slightly weaker correlation is present between M_{BH} and FWHM of the [O III] narrow component.
12. The average inclination of NLSy1 galaxies is lower compared to BLSy1 galaxies. This suggests an inclination as the main geometrical parameter responsible for the black hole mass deficit in NLSy1 galaxies.

We are grateful for the comments and suggestions by the anonymous referee, which helped to improve the manuscript. This work has made use of SDSS spectroscopic data. Funding for SDSS-III has been provided by the Alfred P. Sloan Foundation, the Participating Institutions, the National Science Foundation, and the U.S. Department of Energy Office of Science. The SDSS-III web site is http://www.sdss3.org/. SDSS-III is managed by the Astrophysical Research Consortium for the Participating Institutions of the SDSS-III Collaboration including the University of Arizona, the Brazilian Participation Group, Brookhaven National Laboratory, Carnegie Mellon University, University of Florida, the French Participation Group, the German Participation Group, Harvard University, the Instituto de Astrofisica de Canarias, the Michigan State/Notre Dame/JINA Participation Group, Johns Hopkins University, Lawrence Berkeley National Laboratory, Max Planck Institute for Astrophysics, Max Planck Institute for Extraterrestrial Physics, New Mexico State University, New York University, Ohio State University, Pennsylvania State University, University of Portsmouth, Princeton University, the Spanish Participation Group, University of Tokyo, University of Utah, Vanderbilt University, University of Virginia, University of Washington, and Yale University.

S.R. thanks Neha Sharma (ARIES, India) for carefully reading the manuscript.

References

Abdo, A. A., Ackermann, M., Ajello, M., et al. 2010, ApJS, 188, 405
Alam, S., Albareti, F. D., Allende Prieto, C., et al. 2015, ApJS, 219, 12
Antonucci, R. 1993, ARA&A, 31, 473
Baldi, R. D., Capetti, A., Robinson, A., Laor, A., & Behar, E. 2016, MNRAS, 458, L69
Barrows, R. S., Stern, D., Madsen, K., et al. 2012, ApJ, 744, 7
Bentz, M. C., Denney, K. D., Grier, C. J., et al. 2013, ApJ, 767, 149

Bergeron, J., & Kunth, D. 1984, MNRAS, 207, 263
Bian, W., & Zhao, Y. 2004, MNRAS, 352, 823
Boller, T., Brandt, W. N., & Fink, H. 1996, A&A, 305, 53
Boller, T., Freyberg, M. J., Trümper, J., et al. 2016, A&A, 588, A103
Boroson, T. A. 2002, ApJ, 565, 78
Boroson, T. A., & Green, R. F. 1992, ApJS, 80, 109
Botte, V., Ciroi, S., Rafanelli, P., & Di Mille, F. 2004, AJ, 127, 3168
Bruzual, G., & Charlot, S. 2003, MNRAS, 344, 1000
Calderone, G., Ghisellini, G., Colpi, M., & Dotti, M. 2013, MNRAS, 431, 210
Cappellari, M., McDermid, R. M., Alatalo, K., et al. 2012, Natur, 484, 485
Cavagnolo, K. W., McNamara, B. R., Nulsen, P. E. J., et al. 2010, ApJ, 720, 1066
Condon, J. J. 1992, ARA&A, 30, 575
Cracco, V., Ciroi, S., Berton, M., et al. 2016, arXiv:1607.03438
Dawson, K. S., Schlegel, D. J., Ahn, C. P., et al. 2013, AJ, 145, 10
Decarli, R., Dotti, M., Fontana, M., & Haardt, F. 2008, MNRAS, 386, L15
Ferrarese, L., & Merritt, D. 2000, ApJL, 539, L9
Gaskell, C. M. 1985, ApJ, 291, 112
Gebhardt, K., Bender, R., Bower, G., et al. 2000, ApJL, 539, L13
Goad, M. R., Korista, K. T., & Ruff, A. J. 2012, MNRAS, 426, 3086
Goodrich, R. W. 1989, ApJ, 342, 224
Greene, J. E., & Ho, L. C. 2005, ApJ, 630, 122
Greene, J. E., & Ho, L. C. 2007, ApJ, 670, 92
Grupe, D., Beuermann, K., Mannheim, K., & Thomas, H.-C. 1999, A&A, 350, 805
Grupe, D., & Mathur, S. 2004, ApJL, 606, L41
Jiang, L., Fan, X., Ivezić, Ž, et al. 2007, ApJ, 656, 680
Jun, H. D., Im, M., Lee, H. M., et al. 2015, ApJ, 806, 109
Kaspi, S., Smith, P. S., Netzer, H., et al. 2000, ApJ, 533, 631
Kauffmann, G., Heckman, T. M., Tremonti, C., et al. 2003, MNRAS, 346, 1055
Kellermann, K. I., Sramek, R., Schmidt, M., Shaffer, D. B., & Green, R. 1989, AJ, 98, 1195
Komossa, S., Voges, W., Xu, D., et al. 2006, AJ, 132, 531
Komossa, S., & Xu, D. 2007, ApJL, 667, L33
Kormendy, J., & Ho, L. C. 2013, ARA&A, 51, 511
Kormendy, J., & Richstone, D. 1995, ARA&A, 33, 581
Kovačević, J., Popović, L. Č., & Dimitrijević, M. S. 2010, ApJS, 189, 15
Lawrence, A., Saunders, W., Rowan-Robinson, M., et al. 1988, MNRAS, 235, 261
Leighly, K. M. 1999, ApJS, 125, 317
Liu, X., Yang, P., Supriyanto, R., & Zhang, Z. 2016, IJAA, 6, 166
Luridiana, V., Morisset, C., & Shaw, R. A. 2015, A&A, 573, A42
Magorrian, J., Tremaine, S., Richstone, D., et al. 1998, AJ, 115, 2285
Markwardt, C. B. 2009, in ASP Conf. Ser. 411, Astronomical Data Analysis Software and Systems XVIII, ed. D. A. Bohlender, D. Durand, & P. Dowler (San Francisco, CA: ASP), 251
Marziani, P., Sulentic, J. W., Zwitter, T., Dultzin-Hacyan, D., & Calvani, M. 2001, ApJ, 558, 553
Mathur, S., Kuraszkiewicz, J., & Czerny, B. 2001, NewA, 6, 321
McConnell, N. J., & Ma, C.-P. 2013, ApJ, 764, 184
McIntosh, D. H., Rieke, M. J., Rix, H.-W., Foltz, C. B., & Weymann, R. J. 1999, ApJ, 514, 40
Moran, E. C., Halpern, J. P., & Helfand, D. J. 1996, ApJS, 106, 341
Nandra, K., & Pounds, K. A. 1994, MNRAS, 268, 405
Nelson, C. H., Green, R. F., Bower, G., Gebhardt, K., & Weistrop, D. 2004, ApJ, 615, 652
Netzer, H. 2015, ARA&A, 53, 365
Osterbrock, D. E. 1988, in Active Galactic Nuclei, ed. H. R. Miller & P. J. Wiita (Berlin: Springer), 1
Osterbrock, D. E. 1989, Astrophysics of Gaseous Nebulae and Active Galactic Nuclei (Mill Valley, CA: University Science Books)
Osterbrock, D. E., & Pogge, R. W. 1985, ApJ, 297, 166
Paliya, V. S., Stalin, C. S., & Ravikumar, C. D. 2015, AJ, 149, 41
Pogge, R. W. 2000, NewAR, 44, 381
Rakshit, S., Petrov, R. G., Meilland, A., & Hönig, S. F. 2015, MNRAS, 447, 2420
Richards, G. T., Fan, X., Newberg, H. J., et al. 2002, AJ, 123, 2945
Robson, I. 1996, Active Galactic Nuclei (New York, NY: Wiley)
Rodríguez-Ardila, A., Pastoriza, M. G., & Donzelli, C. J. 2000, ApJS, 126, 63
Ross, N. P., Myers, A. D., Sheldon, E. S., et al. 2012, ApJS, 199, 3
Shen, Y., & Ho, L. C. 2014, Natur, 513, 210
Shen, Y., Richards, G. T., Strauss, M. A., et al. 2011, ApJS, 194, 45
Smith, J. E., Robinson, A., Young, S., Axon, D. J., & Corbett, E. A. 2005, MNRAS, 359, 846
Sulentic, J. W., Marziani, P., Zamanov, R., et al. 2002, ApJL, 566, L71
Tremaine, S., Gebhardt, K., Bender, R., et al. 2002, ApJ, 574, 740
Vanden Berk, D. E., Richards, G. T., Bauer, A., et al. 2001, AJ, 122, 549
Véron-Cetty, M.-P., & Véron, P. 2010, A&A, 518, A10
Véron-Cetty, M.-P., Véron, P., & Gonçalves, A. C. 2001, A&A, 372, 730
Wandel, A. 2002, ApJ, 565, 762
Wandel, A., Peterson, B. M., & Malkan, M. A. 1999, ApJ, 526, 579
Wang, J.-M., Chen, Y.-M., Hu, C., et al. 2009, ApJL, 705, L76
Wang, T., Brinkmann, W., & Bergeron, J. 1996, A&A, 309, 81
Wang, T., & Lu, Y. 2001, A&A, 377, 52
Williams, R. J., Pogge, R. W., & Mathur, S. 2002, AJ, 124, 3042
Woo, J.-H., Schulze, A., Park, D., et al. 2013, ApJ, 772, 49
Woo, J.-H., Treu, T., Barth, A. J., et al. 2010, ApJ, 716, 269
Woo, J.-H., Yoon, Y., Park, S., Park, D., & Kim, S. C. 2015, ApJ, 801, 38
Xiao, T., Barth, A. J., Greene, J. E., et al. 2011, ApJ, 739, 28
Xu, D., Komossa, S., Zhou, H., et al. 2012, AJ, 143, 83
Xu, D., Komossa, S., Zhou, H., Wang, T., & Wei, J. 2007, ApJ, 670, 60
Yuan, W., Zhou, H. Y., Komossa, S., et al. 2008, ApJ, 685, 801
Zakamska, N. L., Strauss, M. A., Krolik, J. H., et al. 2003, AJ, 126, 2125
Zhang, T.-Z., & Wu, X.-B. 2002, ChJAA, 2, 487
Zhang, X.-G. 2014, MNRAS, 438, 557
Zhang, X.-G., & Feng, L.-L. 2016, MNRAS, 457, 3878
Zhou, H., Wang, T., Yuan, W., et al. 2006, ApJS, 166, 128